

M2 de la Spécialité Océan, Atmosphère, Climat et Télédétection

Variabilité climatique dans les tropiques

Claude Frankignoul

Université Pierre et Marie Curie

TABLE DES MATIERES

1. INTRODUCTION

- 1.1 Circulation océanique tropicale
- 1.2 Circulation atmosphérique tropicale
- 1.3 ENSO et la variabilité climatique

2. LES ONDES EQUATORIALES

- 2.1 Les équations du mouvement
- 2.2 Modes normaux
- 2.3 Les différents types d'onde
- 2.4 Réflexion des ondes océaniques
- 2.5 Observations

3. REPONSE DE L'OCEAN AU FORGAGE ATMOSPHERIQUE

- 3.1 Variations de la température océanique superficielle
- 3.2 Ajustement océanique

4. REPONSE DE L'ATMOSPHERE AU FORCAGE OCEANIQUE

- 4.1 L'atmosphère tropicale
- 4.2 Ondes atmosphériques équatoriales
- 4.3 Réponse de l'atmosphère à un échauffement diabatique
- 4.4 Influence des anomalies de température océanique superficielle

5. DYNAMIQUE DU SYSTEME COUPLE OCEAN-ATMOSPHERE

- 5.1 El Niño et Oscillation du Sud
- 5.2 La théorie de l'oscillateur retardé
- 5.3 Influence des non-linéarités et du cycle saisonnier
- 5.4 Prévisibilité climatique

Appendix : Empirical orthogonal functions et maximum covariance analysis

TRAVAUX PRATIQUES:

Lecture et présentation d'articles

BIBLIOGRAPHIE

- Gill, A.E., 1982 : Atmosphere-ocean dynamics. Academic Press, 662 p.
- Marshall, J. and R.A. Plumb, 2008 : Atmosphere, ocean, and climate dynamics : an introductory text. Elsevier, 319 p.
- Pedlosky, J., 1987 : Geophysical Fluid Dynamics. Springer-Verlag, 710 p.
- Pedlosky, J., 2003 : Waves in the ocean and atmosphere. Springer-Verlag, 260 p.
- Philander, S.G., 1990: El Niño, La Niña, and the Southern Oscillation. Academic Press, Inc., 293 p.
- Sarachick, E.S. and M.J. Cane, 2010 : The El Niño-Southern Oscillation phenomenon, Cambridge University Press, ISBN 978-0-521-84786-5

Informations, animations, observations et prévisions à :

- <http://www.pmel.noaa.gov/tao/elnino/nino-home.html#>
- <http://www.cdc.noaa.gov/people/joseph.barsugli/anim.html>
- <http://www.cgd.ucar.edu/cas/ENSO/enso.html>
- <http://www.pmel.noaa.gov/tao/jsdisplay/monthly-summary/monthly-summary.html>
- <http://sealevel.jpl.nasa.gov/science/jason1-quick-look/>
- http://www.cpc.ncep.noaa.gov/products/Global_Monsoons/Global-Monsoon.shtml
- http://iri.columbia.edu/climate/ENSO/currentinfo/SST_table.html
- http://www.ecmwf.int/products/forecasts/d/charts/seasonal/forecast/seasonal_range_forecast/
- http://www.cpc.ncep.noaa.gov/products/analysis_monitoring/enso_advisory/ensodisc.html
- <http://www.cpc.ncep.noaa.gov/products/precip/CWlink/MJO/enso.shtml>
- <http://www.ncdc.noaa.gov/oa/climate/research/sst/clim.php>

1. INTRODUCTION

Le comportement du système océan - atmosphère dans les régions tropicales est différent de celui des latitudes extratropicales, à cause de changements fondamentaux dans la dynamique et la thermodynamique des deux milieux. Lorsqu'on s'approche de l'équateur, la force de Coriolis tend vers zéro et la contrainte géostrophique se relâche. La diminution du paramètre de Coriolis f entraîne une augmentation de la vitesse de propagation des ondes de Rossby et l'apparition de nouveaux types d'ondes, en particulier l'onde de Kelvin équatoriale, qui se propage très rapidement le long de l'équateur. L'augmentation de la vitesse de propagation des ondes de Rossby se voit aisément dans le cas des ondes longues dont la fréquence dans le plan β est donnée par $\omega = -\beta k c_n^2 f^{-2}$ où $c_n = (gh_n)^{1/2}$ est la vitesse d'une onde de gravité et h_n la profondeur équivalente. Lorsque la latitude diminue, la vitesse de propagation ω/k augmente approximativement comme f^{-2} . Ainsi, un premier mode barocline qui se propage à quelques cm/s dans les latitudes tempérées le fait à plus de 50 cm/s lorsqu'on s'approche de l'équateur (figure de Chelton et Schlax, Science 1996).

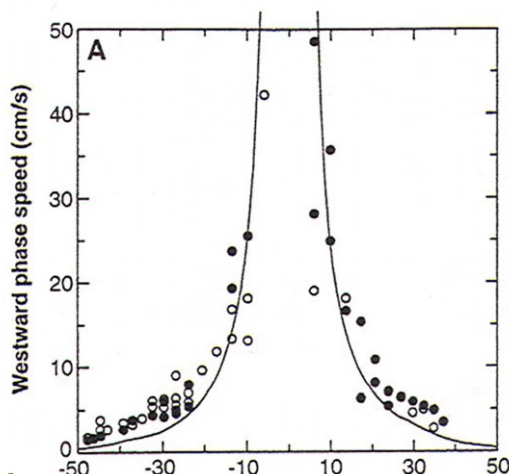


Fig. 5. (A) Globally distributed estimates of the phase speeds of westward-propagating sea level signals estimated from 3 years of TOPEX/POSEIDON altimeter observations. The solid circles correspond to Pacific estimates, and the open circles correspond to Atlantic and Indian Ocean estimates. The global average latitudinal variation of the phase speed predicted by the standard theory for extratropical freely propagating, nondispersive, linear, first-mode baroclinic Rossby waves (10) is superimposed as the continuous line.

La propagation vers l'ouest des ondes de Rossby longues est illustrée ci-dessous à partir des observations altimétriques de TOPEX/POSEIDON (Leeuwenburgh and Stammer, JPO 2001). En haut, anomalies de l'élévation de la surface libre par rapport au signal saisonnier. En bas, la même chose après filtrage éliminant les longueurs d'onde > 4000 km et les périodes beaucoup plus courtes que celles des ondes de Rossby baroclines à chaque latitude. On notera que les ondes se propagent beaucoup plus rapidement à basse latitude.

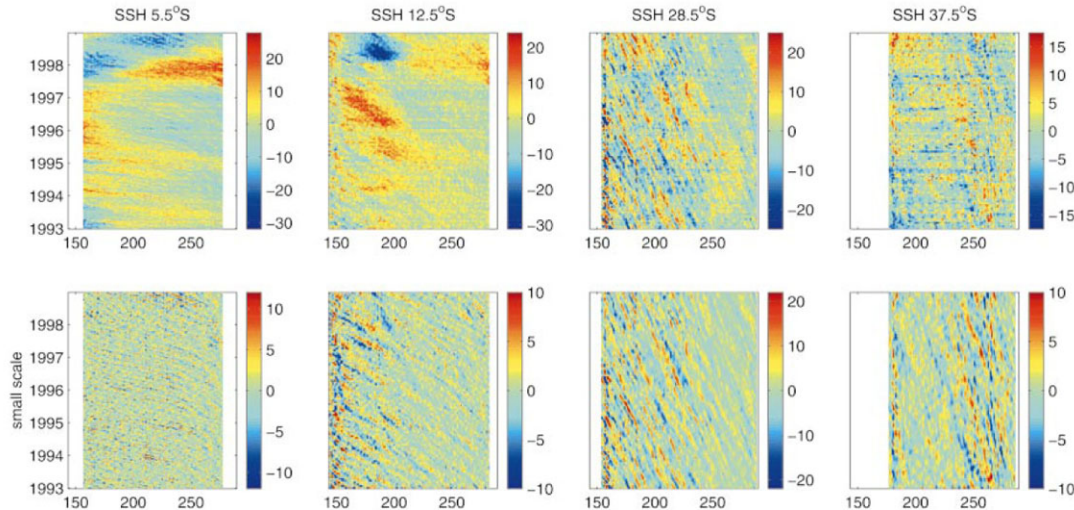


FIG. 9. Time-longitude sections of η' along various latitudes in the South Pacific: 5.5°S , 12.5°S , 25.5°S , and 37.5°S .

Un premier mode barocline de Rossby traverse l'océan Pacifique en 6 mois. Il existe un autre type d'onde, l'onde de Kelvin équatoriale, qui est encore plus rapide et traverse le Pacifique en 2 mois. A l'équateur, le temps d'ajustement de l'océan à un changement de vent dépend de la propagation de ces deux types d'onde et est beaucoup plus court qu'aux latitudes tempérées. L'océan équatorial peut ainsi répondre à des variations relativement rapides du forçage atmosphérique et l'on observe en effet de fortes variations saisonnières et interannuelles des courants équatoriaux. Par contre, la réponse océanique sera plus lente dès qu'on s'éloigne de l'équateur. Cette dépendance latitudinale a une forte influence sur la variabilité interannuelle du système tropical.

Sauf très près de l'équateur, les courants océaniques obéissent à une dynamique semblable à celle qui régit les courants des latitudes extratropicales. Ainsi, le Contre courant équatorial nord (voir sketch ci-dessous, de Philander 1990) résulte d'un changement de signe du pompage d'Ekman au sud de la gyre subtropicale. Les courants tropicaux ont de fortes variations saisonnières et interannuelles, mais elles s'expliquent aisément par les variations correspondantes de la tension de vent. Par

contre, près de l'équateur, la dynamique des courants loin du bord ouest devient beaucoup plus complexe qu'une simple dynamique quasi-géostrophique linéaire. En particulier, les termes non linéaires et la dissipation jouent un rôle très important dans la génération du Sous-courant équatorial que l'on observe le long de l'équateur dans le Pacifique et l'Atlantique. Enfin, on notera qu'il y a upwelling le long de l'équateur à cause de la divergence des courants d'Ekman dans la couche de surface (à droite du vent dans l'hémisphère nord et à gauche dans l'hémisphère sud)

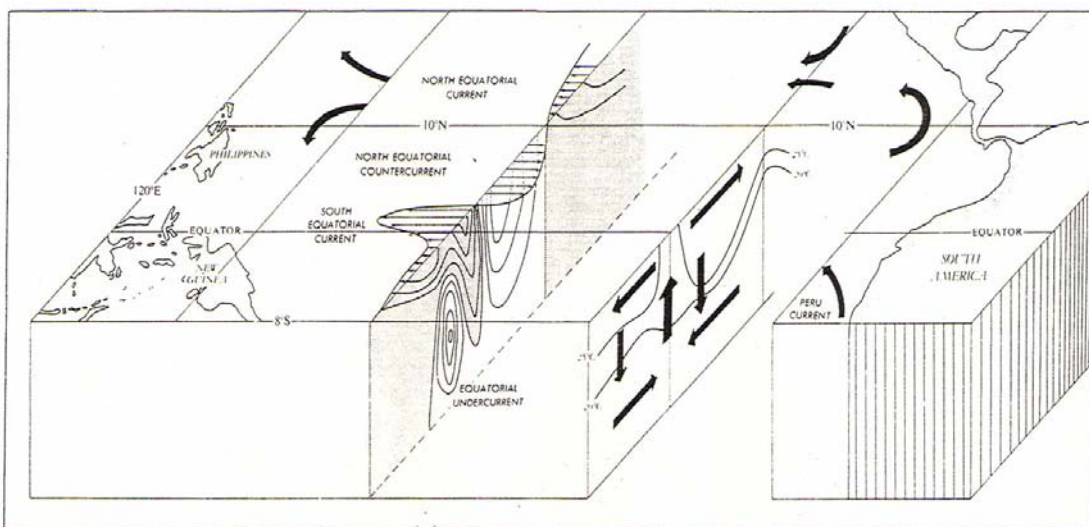


Figure 2.1. A schematic diagram of the horizontal and vertical circulation in the tropical Pacific Ocean.

engendrés par les vents alizés. Néanmoins, la circulation des couches supérieures de l'océan équatorial est largement déterminée par les variations de la tension de vent. Le schéma ci-dessous (Wyrtki, JPO 1974) illustre la forte variabilité saisonnière du système de courant dans le Pacifique tropical.

Les conditions climatologiques pour la température de surface dans le Pacifique Tropical montrent que la température superficielle de l'océan est maximale légèrement au nord de l'équateur. Dans la partie est du bassin, elle est moins élevée à l'équateur, à cause de l'upwelling équatorial causé par les vents d'est. Celui-ci est responsable du fort gradient zonal de température. La circulation atmosphérique est très fortement influencée par la distribution de la température de surface de l'océan. En effet, la convection cumulus apparaît au-dessus des eaux les plus chaudes, où l'évaporation et la pluviosité sont très fortes, conduisant à des régions de forte convergence des vents de surface, notamment le long des zones de convergence intertropicale (ITCZ). Les zones de forte convection contribuent à la composante

zonalement symétrique de la circulation atmosphérique (cellule de Hadley) et contrôlent ses composantes zонаlement asymétriques (circulation de Walker).

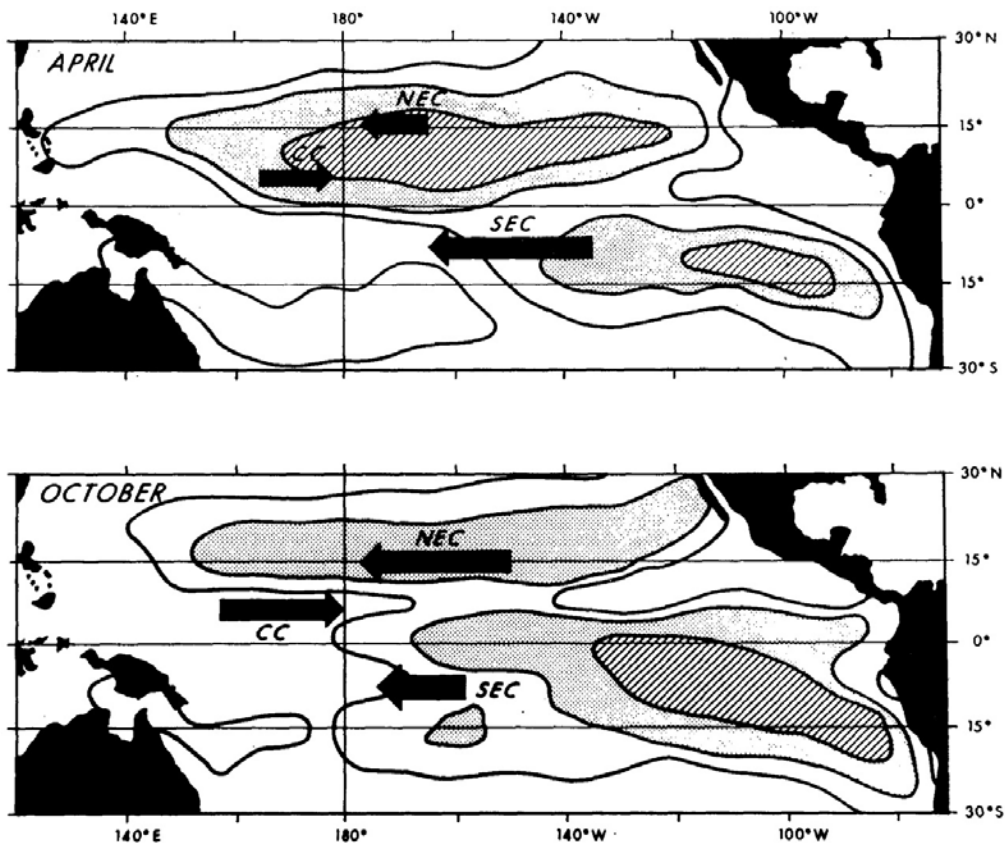
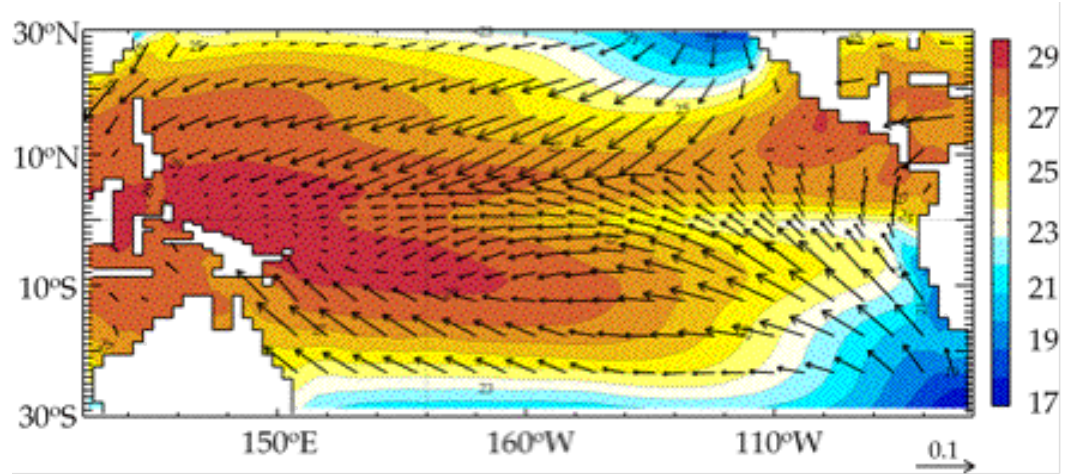


FIG. 7. Strength of equatorial currents in relation to the trade wind systems in April and October. Maps of the constancy of trade winds are according to Crowe (1951a), giving areas of 50%, 70% and 90% constancy of direction. Strength of currents is shown by relative length of arrows. NEC = North Equatorial Current, CC = Countercurrent, SEC = South Equatorial Current.



Climatologie de la température de surface et du vent dans le Pacifique tropical.

Comme la convection cumulus et l'atmosphère tropicale répondent rapidement à un changement de température de l'océan et que celle-ci varie avec la saison, la circulation atmosphérique a un cycle saisonnier important illustré ci-dessous pour la

circulation de surface (Fig. 2) et la cellule de Hadley dont la branche ascendante est dans l'hémisphère d'été (figure 7.19 de Peixoto et Oort, 1992).

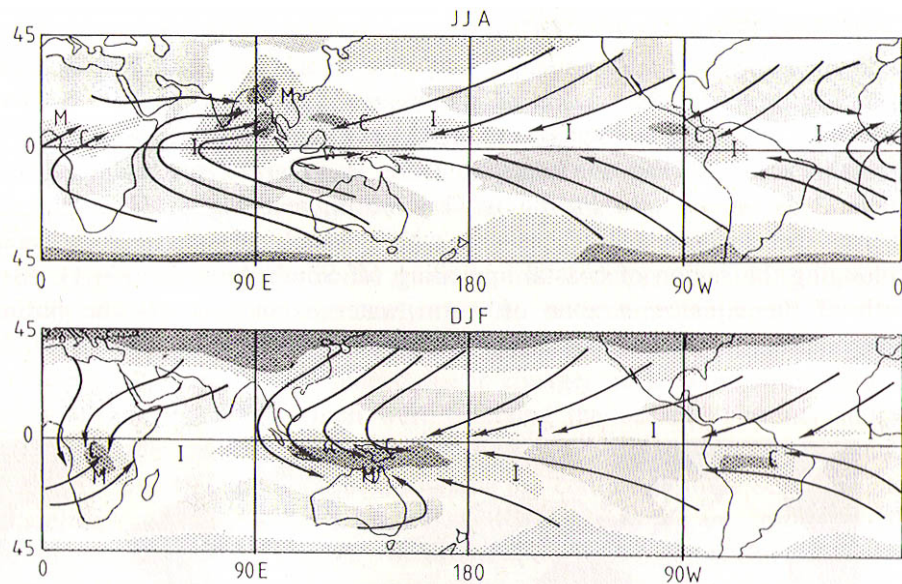


Fig. 2. Schematic view of the atmospheric surface circulation of the tropics for the boreal summer (top) and winter (bottom). Contours show the long-term mean longwave radiation to space. Low radiating regions are indicated, with the darkest shading indicating the regions of most persistent and intense convection (radiation increases from dark, stippled, clear to grey). Label I, C and M show the location of the intertropical convergence zone, the semi-permanent equatorial convective zones and the seasonal monsoon regions, respectively. The solid lines indicate the monsoonal and near-equatorial flow. Adapted from Webster (1983).

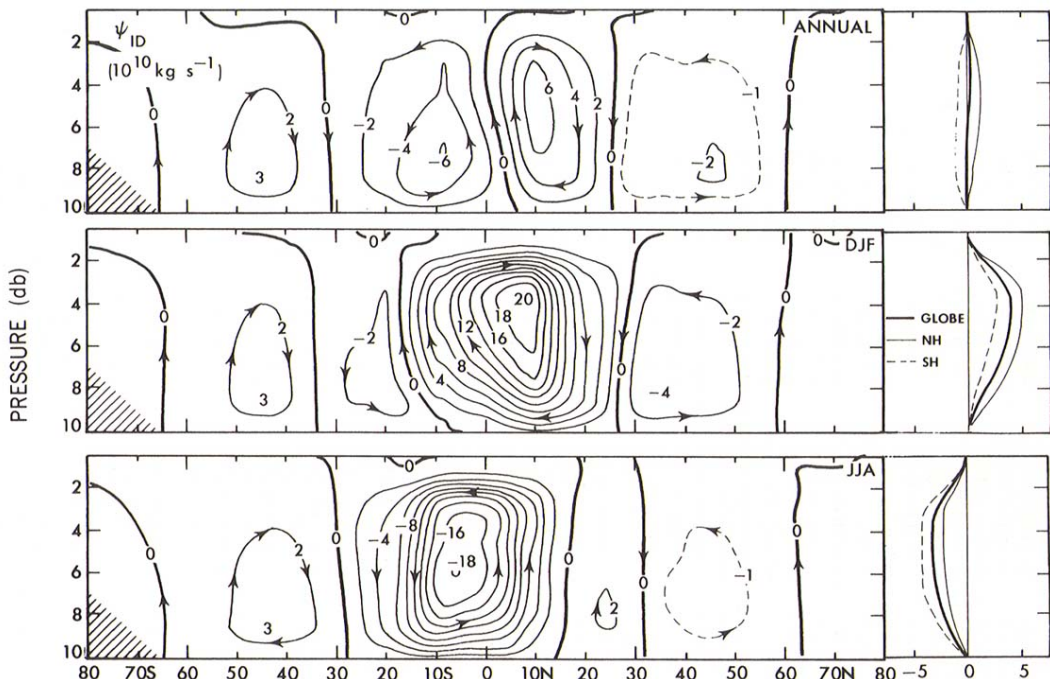


FIGURE 7.19. Zonal-mean cross sections of the mass stream function in $10^{10} \text{ kg s}^{-1}$ for annual, DJF, and JJA mean conditions. Vertical profiles of the hemispheric and global mean values are shown on the right.

La circulation de Walker (comme l'a nommée Bjerknes) consiste principalement en deux cellules longitudinales équatoriales, l'une au-dessus du Pacifique et l'autre au-dessus de l'océan Indien. Elle est causée par la forte évaporation et l'intense convection qui a normalement lieu au-dessus des eaux chaudes qui se trouvent l'ouest de ces deux océans tropicaux. La chaleur libérée dans ces zones de forte pluie entraîne une dépression des surfaces isobares et crée une zone de basse pression. A l'est de cette zone, la température de l'océan est plus basse, la convection moindre ou absente, et la pression est plus haute. Ce sont des zones de subsidence. En l'absence de forces de Coriolis, la différence de pression qui en résulte entraîne le vent de surface vers la zone de convection. Il y a divergence en altitude et la circulation est fermée, du moins à l'équateur, par un vent zonal de direction opposée à celle du vent de surface. En surface, le vent d'est associé à la circulation de Hadley est donc renforcé dans le Pacifique Tropical. Il y a également une cellule de Walker dans l'Atlantique Tropical, avec forte convection au-dessus de l'Amazone. Enfin, il y a des cellules qui sont fonction du contraste océan - continent et varient avec la saison. Elles sont liées aux moussons, qui jouent un rôle climatique très important par les variations de pluviosité qui leur sont associées.

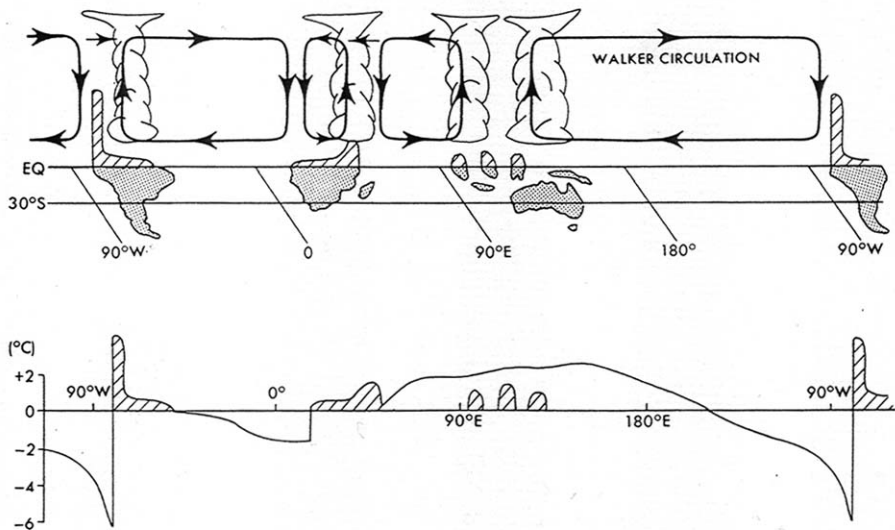


FIGURE 16.5. Schematic diagram of the normal Walker circulation along the equator during non-ENSO conditions. Rising air and heavy rains tend to occur over Indonesia and the western Pacific, southeast Africa, and the Amazon area in South America, while sinking air and desert conditions prevail over the eastern equatorial Pacific and southwest Africa (see also Fig. 7.24). The strongest branch of the Walker circulation over the Pacific is related to the very warm SST in the west Pacific where the air is rising, and the cool SST in the east Pacific where the air is sinking. The SST departures from the zonal-mean along the equator are shown in the lower part of the figure (after Wyrtki, 1982).

Une vue plus détaillée des circulations de Hadley et de Walker dans le Pacifique est donnée ci-dessous pour le mois de janvier (Wang, J. Climate 2002), faisant apparaître une complexité qui est quelque peu masquée par le schéma ci-dessus. On notera qu'une zone de convergence dans la basse troposphère correspond à une zone de divergence dans la haute troposphère, ainsi qu'à un mouvement ascendant. La vitesse verticale à 500 mb montre clairement la position de la zone intertropicale de convergence (ITCZ) qui est vers 10°N à l'est du Pacifique et est associée à une température de surface de la mer élevée, une bande étroite de convection et un mouvement ascendant. On voit également la zone de convergence du Pacifique Sud-ouest. Notons aussi la grande zone de subsidence dans les latitudes tempérées à l'ouest du continent américain (subtropical high). La figure suivante montre que la circulation « locale » de Hadley (i.e. la circulation atmosphérique prise en moyenne zonale sur une région limitée) est différente dans le Pacifique ouest et le Pacifique est, reflétant en partie la distribution différente de la température océanique de surface.

Les forts vents alizés ont un impact important sur la circulation océanique car la tension turbulente engendrée par le vent est principalement équilibrée par un gradient zonal de pression dans la partie supérieure de l'océan. Ainsi, en conditions climatologiques, l'ouest du Pacifique est environ 40 cm plus haut que l'est. Le gradient de l'élévation du niveau de la mer est compensé par une pente opposée de la thermocline, qui est normalement assez profonde à l'ouest (warm pool), mais proche de la surface à l'est (Fig.1 de Watanabe JCLI 2008). L'upwelling équatorial dû aux vents alizés refroidit donc aisément la zone équatoriale au centre et, surtout, à l'est du Pacifique où il crée une « langue froide équatoriale ». A l'ouest, l'upwelling équatorial ne ramène en surface que des eaux chaudes. Le gradient zonal de température maintient les vents alizés, qui maintiennent le gradient zonal de température. Le système océan - atmosphère semble donc en équilibre. Cependant, les observations montrent qu'il y a toujours d'importantes fluctuations saisonnières et interannuelles. Notons que la situation est semblable dans l'Atlantique Tropical.

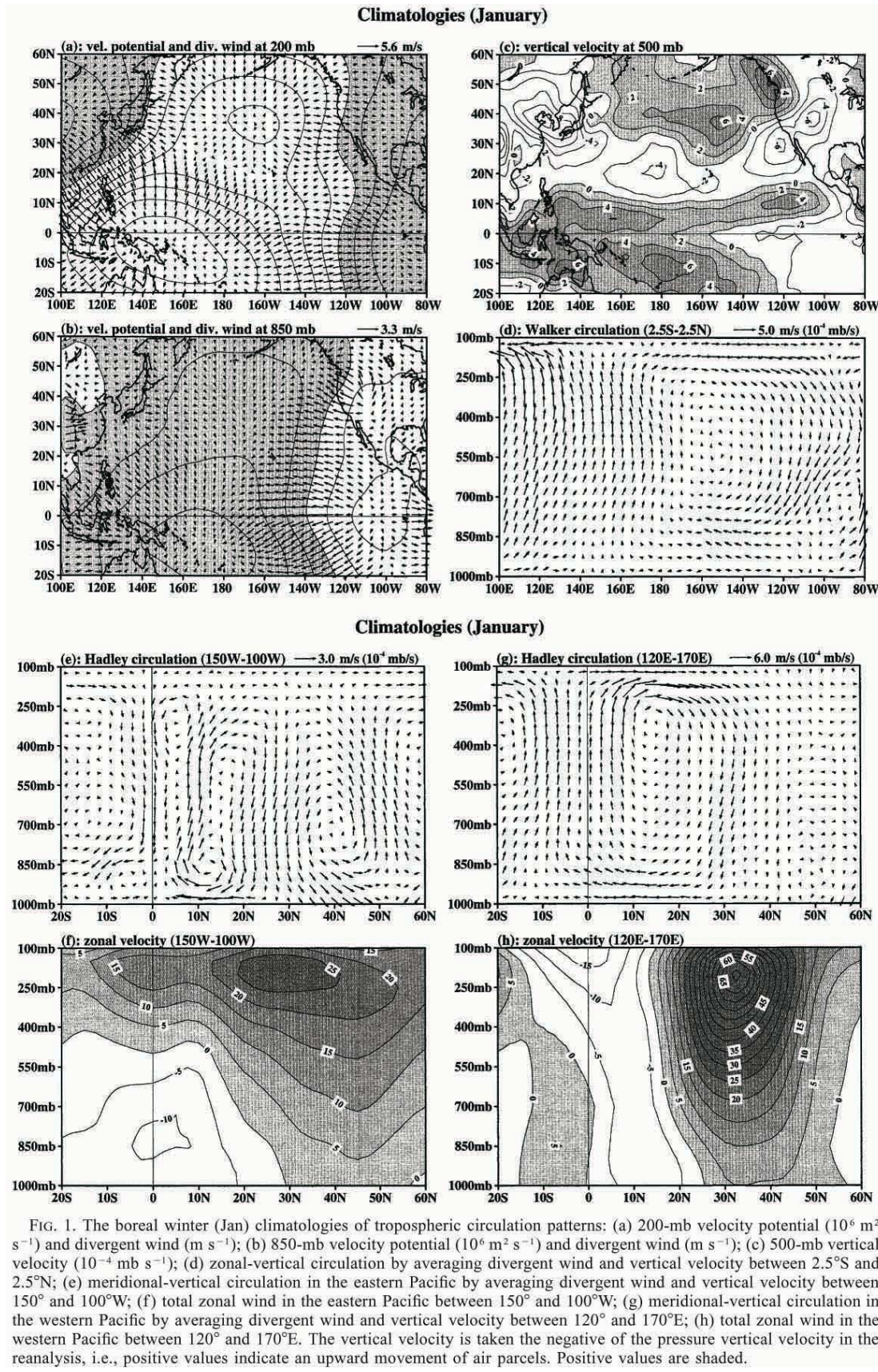


FIG. 1. The boreal winter (Jan) climatologies of tropospheric circulation patterns: (a) 200-mb velocity potential ($10^6 \text{ m}^2 \text{ s}^{-1}$) and divergent wind (m s^{-1}); (b) 850-mb velocity potential ($10^6 \text{ m}^2 \text{ s}^{-1}$) and divergent wind (m s^{-1}); (c) 500-mb vertical velocity ($10^{-4} \text{ mb s}^{-1}$); (d) zonal-vertical circulation by averaging divergent wind and vertical velocity between 2.5°S and 2.5°N ; (e) meridional-vertical circulation in the eastern Pacific by averaging divergent wind and vertical velocity between 150° and 100°W ; (f) total zonal wind in the eastern Pacific between 150° and 100°W ; (g) meridional-vertical circulation in the western Pacific by averaging divergent wind and vertical velocity between 120° and 170°E ; (h) total zonal wind in the western Pacific between 120° and 170°E . The vertical velocity is taken the negative of the pressure vertical velocity in the reanalysis, i.e., positive values indicate an upward movement of air parcels. Positive values are shaded.

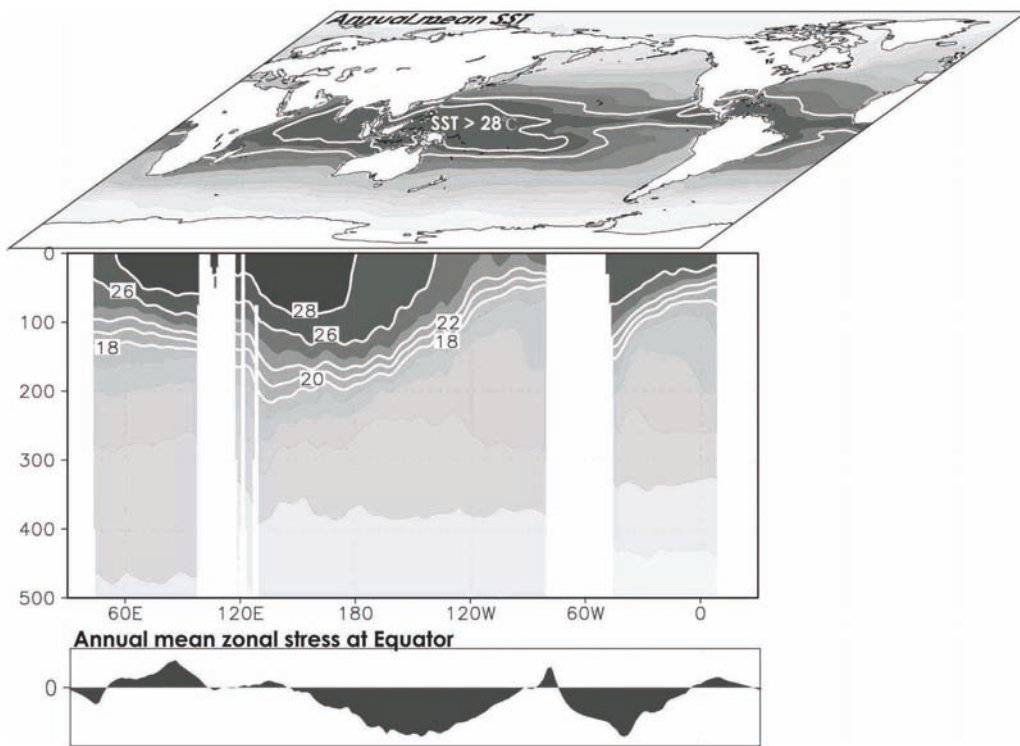


FIG. 1. Annual mean climatology of (top) SST, (middle) subsurface temperature, and (bottom) zonal stress along the equator. The contours of 26°C (28°C) are indicated in the top panel.

Vu l'échelle de temps très courte de la convection, l'atmosphère réagit fortement et rapidement aux changements de la température de surface de l'océan. Bien que l'atmosphère tropicale ait une certaine variabilité intrinsèque (dont l'existence est indépendante des conditions en surface), les caractéristiques principales de la circulation atmosphérique tropicale, en particulier la tension de vent, sont essentiellement déterminées par la température de surface de l'océan et des continents aux échelles de temps supérieures à un mois ou deux. Cependant, les fluctuations atmosphériques et en particuliers les ondes de Madden et Julian et les coups de vent d'ouest qui leur sont associés jouent le rôle d'un forçage stochastique de la variabilité à plus longue échelle de temps. L'océan répond aux changements de la tension de vent. Cependant, l'intérieur de l'océan répond plus lentement que sa surface, et ce d'autant plus qu'on est loin de l'équateur, ce qui fait qu'à l'échelle saisonnière et interannuelle l'océan n'est pas en équilibre avec l'atmosphère, surtout dans le Pacifique. Néanmoins, chaque milieu est fortement contrôlé par l'autre et les deux milieux varient principalement aux mêmes échelles de temps. Ceci diffère des régions extratropicales où le couplage entre l'océan et l'atmosphère est faible et les échelles de temps dominantes sont différentes dans les deux milieux. En effet, dans les moyennes et hautes latitudes, l'atmosphère ne répond que de façon limitée aux

changements de la température de surface de l'océan, et elle a une très forte variabilité intrinsèque à courte échelle de temps (les variations du temps). Dans ce cas, l'océan répond en intégrateur, favorisant ainsi les longues échelles de temps.

Le fort couplage entre l'océan et l'atmosphère des basses latitudes explique pourquoi les variations climatiques les plus importantes que l'on rencontre aux échelles de temps allant du mois à plusieurs décennies sont causées par les tropiques. Le phénomène climatique le plus spectaculaire est connu sous le nom de El Niño Oscillation Australe (El Niño Southern Oscillation ou ENSO) qui a son origine dans le couplage entre l'océan et l'atmosphère dans le Pacifique tropical. L'Oscillation Australe (Walker 1923) décrit l'importante bascule de la pression atmosphérique entre l'Est et l'Ouest du Pacifique que l'on observe aux échelles interannuelles et qui correspond à une modification de la cellule de Walker et, dans moindre mesure, de la cellule de Hadley. Walker avait observé qu'une forte pression à Tahiti s'accompagnait d'une basse pression à Darwin en Australie, et avait défini l'indice de l'Oscillation Australe comme étant la différence de pression entre Darwin et Tahiti. Les observations montrent que l'Oscillation Australe a une très grande échelle et s'étend principalement sur tout le Pacifique, y affectant en particulier le champ de vent (Fig. 1.1 ci-dessous).

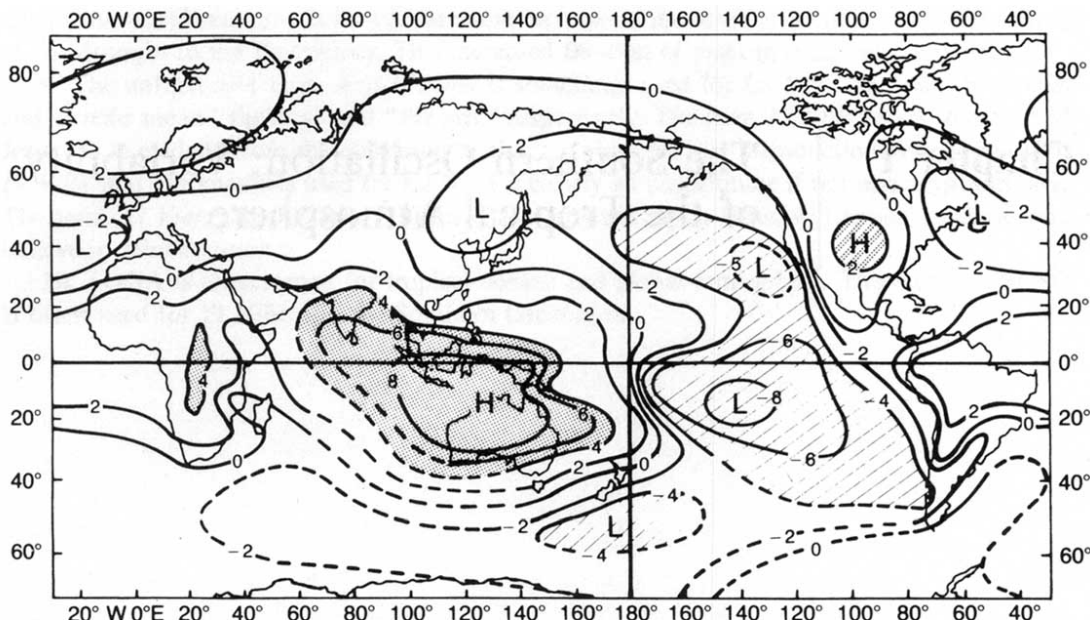
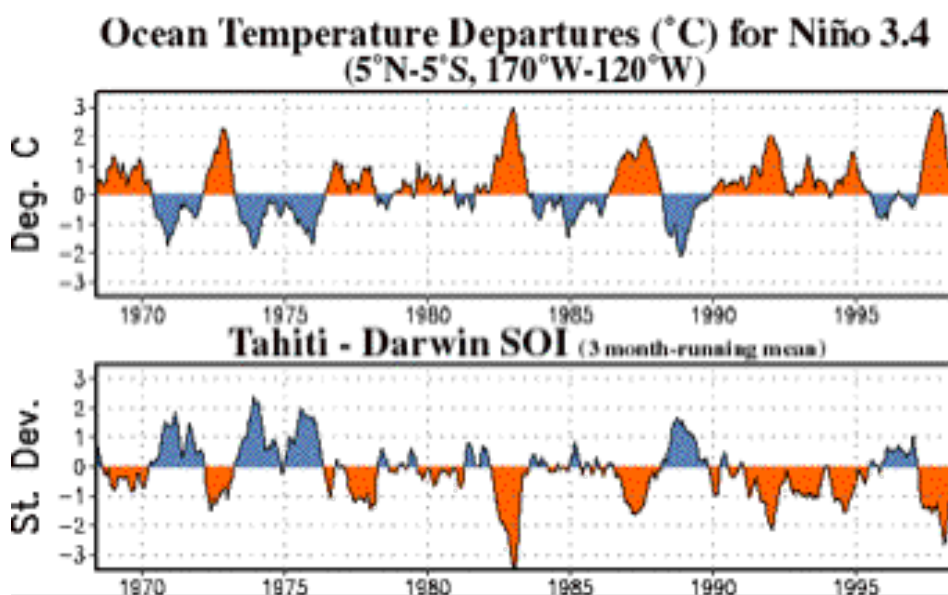


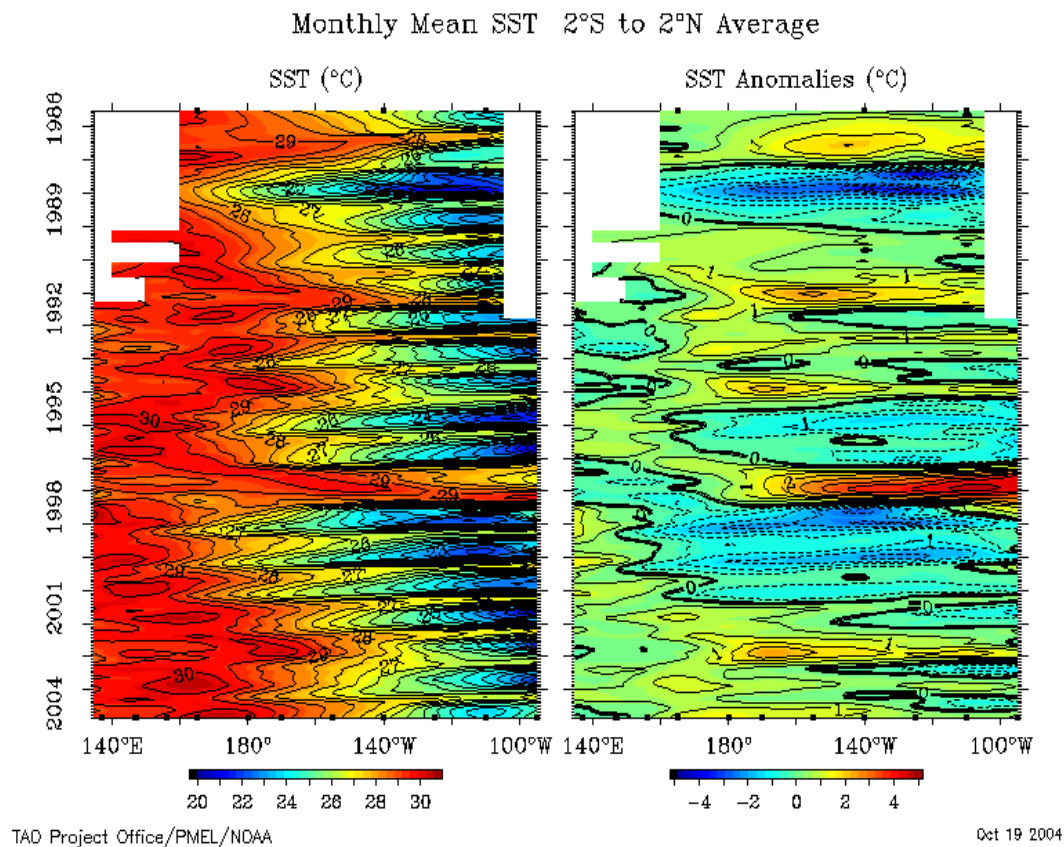
Figure 1.1. Correlations ($\times 10$) of annual mean sea level pressure with the pressure at Darwin. Correlations exceed 0.4 in the shaded regions and are less than -0.4 in the regions with dashed lines. [From Trenberth and Shea (1987).]

Bjerknes (1969) a fait le lien entre les variations de l'Oscillation Australe et la température de la surface de l'océan équatorial au large du Pérou, qui augmente fortement tous les trois à cinq ans en moyenne (phénomène El Niño) lorsque l'Oscillation Australe est négative, entraînant des modifications globales du climat. Le phénomène El Niño est illustré en contrastant la température de surface en novembre 1982 (au pic d'un des très grands événements ENSO du 20^{ème} siècle) et novembre 1983. La figure suivante illustre l'irrégularité du phénomène. On notera l'importance de l'El Niño de 1998-1999, qui est le plus fort événement depuis qu'il y a des mesures instrumentales. Enfin, l'influence de El Niño sur la pluviosité, la température de l'air et la circulation atmosphérique est esquissée plus bas (Liu and Alexander 2007). On notera les zones de sécheresse ou de pluie torrentielle, ainsi que les téléconnexions avec les moyennes et hautes latitudes via la « Pacific North American pattern ».



Si l'Oscillation Australe varie essentiellement en réponse aux changements de la température superficielle du Pacifique équatorial, la température océanique superficielle est largement influencée par la réponse de l'océan au forçage par le vent et dépend donc de l'Oscillation Australe. Lors d'un événement La Niña (eaux anormalement froides le long de l'équateur), le gradient zonal de température superficielle est plus important et les vents alizés sont plus forts. En conséquence, la thermocline est beaucoup plus profonde à l'ouest du Pacifique, où il y a une énorme quantité d'eau chaude, la « warm pool », qu'à l'est où elle est très proche de la

surface. Ceci favorise l'upwelling équatorial et maintient le fort gradient de température est-ouest. C'est une situation apparemment stable. Par contre, durant El Niño, la thermocline est à peu près à la même profondeur tout au long de l'équateur et les eaux chaudes s'étendent sur tout le bassin équatorial, entraînant avec elles le



TAD Project Office/PMEL/NOAA

Oct 19 2004

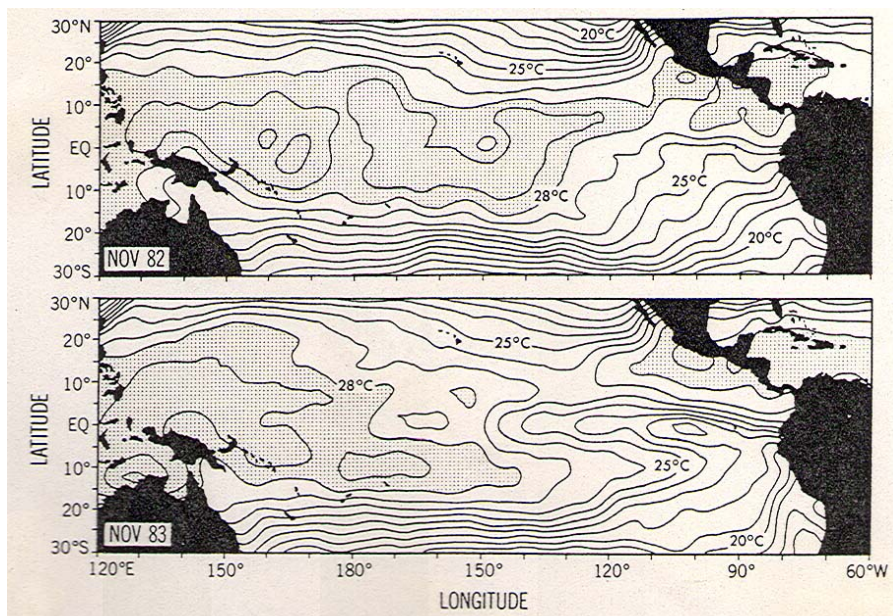


Figure 1.13. Sea surface temperatures in November 1982 during El Niño and one year later during La Niña.

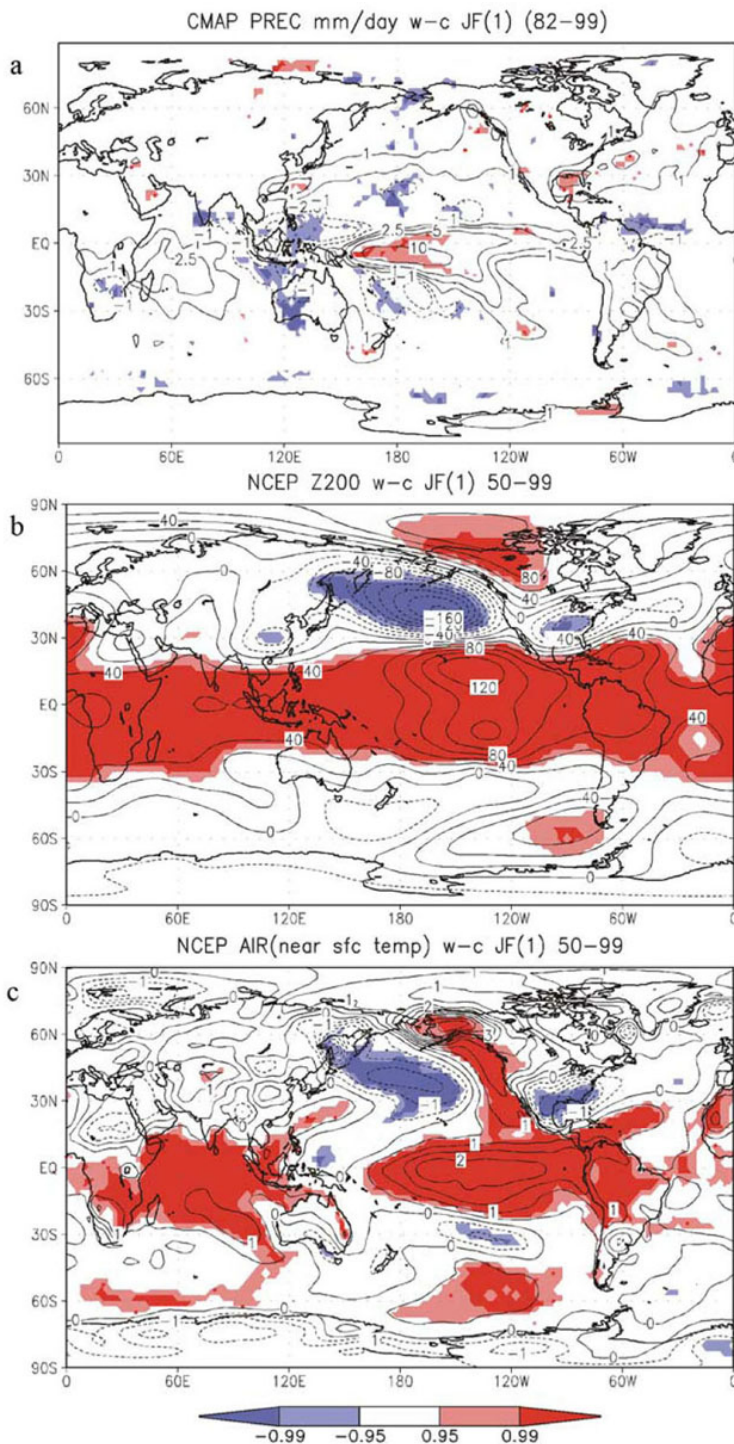
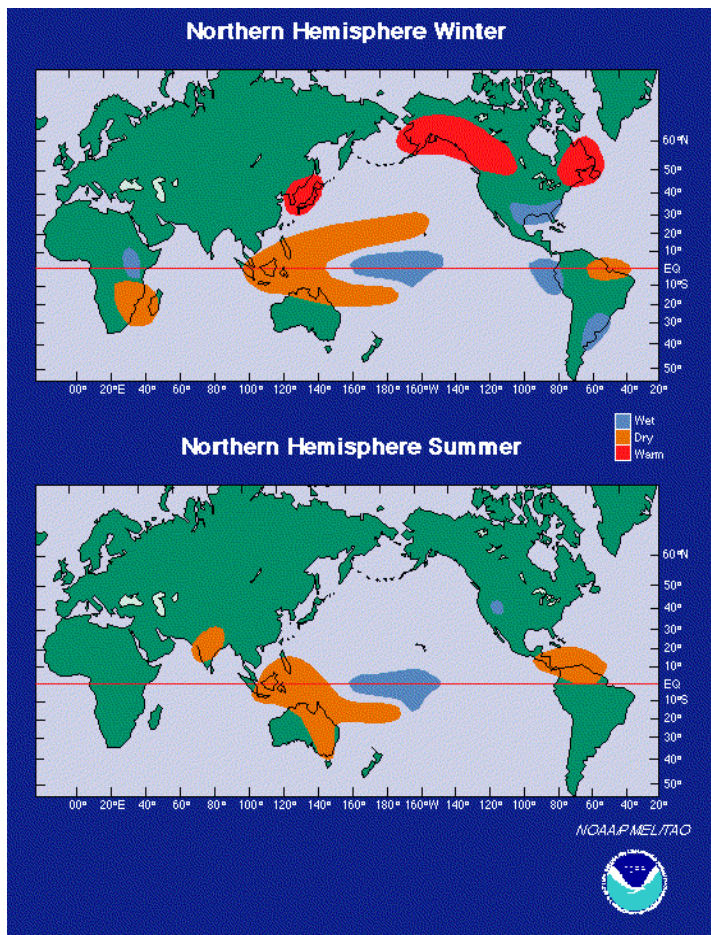


Figure 3. El Niño (warm)–La Niña (cold) composite average of (a) precipitation (shaded interval is 0.25 mm d^{-1} , contours at $\pm 1, 2.5, 5.0$, and 10.0 mm d^{-1}), (b) 200 mb height (contour interval 20 m), and (c) near-surface air temperature during January and February (JF), where 0 indicates the year ENSO peaks and 1 indicates the following year. Shading indicates areas where the warm and cold composites are significantly different from each other at the 95% and 99% level as indicated by Monte Carlo resampling of the composite members. During El Niño events the precipitation is enhanced above and to the west of the anomalously warm water in the equatorial Pacific. The associated heating warms the tropical atmosphere and drives stationary patterns and storm track anomalies. The latter is indicated by the precipitation changes over the North Pacific and North Atlantic oceans. These ENSO-induced atmospheric changes force SST anomalies to form over the global oceans. The precipitation values are from the Climate Prediction Center Merged Analysis of Precipitation (CMAP) data set [Xie and Arkin, 1997] for ENSO events that occurred between 1979 and 2000, and the heights and temperature are from NCEP reanalysis for events between 1950 and 2000.



zones de forte convection qui se déplacent vers l'est. L'affaissement du gradient zonal de température océanique superficielle affaiblit la cellule de Walker, diminue ou même renverse les vents alizés et réduit l'influence de l'upwelling équatorial à l'est, puisqu'il n'amène plus d'eau froide en surface. C'est à nouveau une situation qui devrait être stable. Pourtant, le système océan – atmosphère n'est pas dans un état d'équilibre. La question est donc de comprendre ce qui perturbe suffisamment le système pour qu'il ne reste pas dans un état stable. On verra qu'un équilibre ne peut être atteint à cause de la réponse lente de l'intérieur de l'océan au forçage atmosphérique et que le cycle saisonnier joue également un rôle. En outre, les ondes de Madden-Julian agissent comme un forçage stochastique. Il en résulte un comportement irrégulier, mais qui a une prévisibilité relativement importante qui est maintenant utilisée en routine à des fins socio-économiques.

Notons qu'un fort couplage entre l'océan et l'atmosphère est également observé dans l'océan Atlantique équatorial, mais à cause de la plus petite dimension du bassin, il ne donne pas naissance à un phénomène aussi spectaculaire que ENSO.

Enfin, le couplage air-mer est aussi très important, mais différent, dans l'océan Indien, où il joue un rôle important dans la mousson.

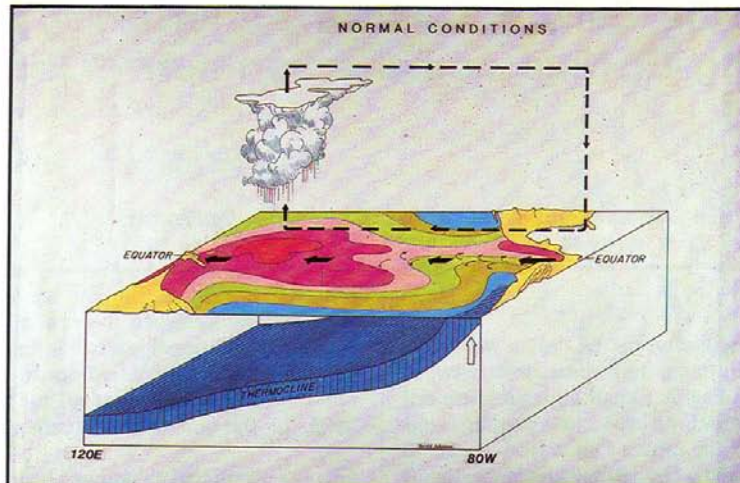


Figure 1: Schematic of the Normal Conditions Prevailing in the Equatorial Pacific. The region is characterized by trade winds blowing east-to-west across the basin. Rising motion, active convection, and heavy rainfall occur over the warm sea surface temperatures in the west. The trade winds converge into this region at the surface, and at upper levels the flow is reversed. The effect of the surface winds on the ocean is to induce upwelling along the equator, and to force the surface waters westward, so that the colder abyssal waters are brought close to the surface in the east, and are depressed in the west. The thermocline, which divides the near-surface waters from the abyssal waters, is thus shallow in the east and deep in the west. Because of the shallow thermocline and equatorial upwelling in the east Pacific, the sea surface temperatures are relatively cool there. These states of the equatorial ocean and atmosphere are mutually reinforcing. That is, the east-to-west temperature difference which acts to drive the trade winds is itself set up by the trade winds.

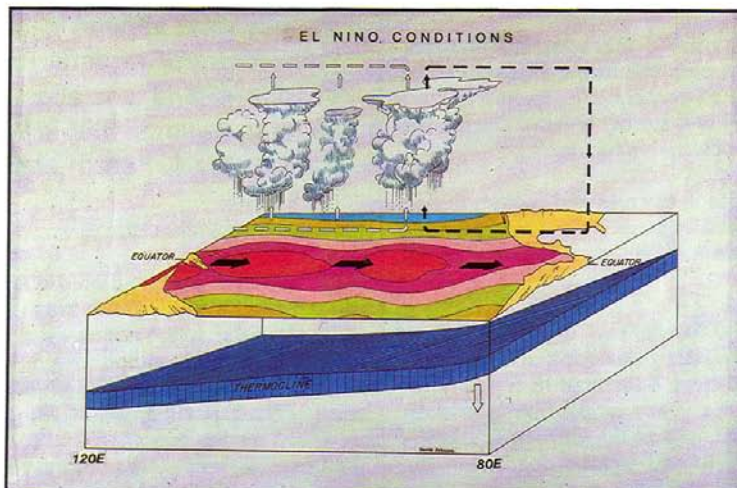


Figure 2: Schematic of El Niño Conditions. In this state, large changes in both the atmospheric and oceanic patterns are seen. The equatorial trade winds relax, and sometimes even reverse, in the western and central regions. This occurs in association with a warming of central and east Pacific sea surface temperatures, and the expansion of the convective region eastward into the central Pacific. The weakened trades cause an eastward displacement of the warm surface waters of the west Pacific, and a reduction in equatorial upwelling, both of which act to induce warming in the east Pacific. Once again, these changes are mutually reinforcing, allowing a sustained episode of anomalous conditions.

2. Equatorial waves

a Equations of motion. Although most numerical models use the spherical coordinates, tropical motions are most easily described in the equatorial β -plane. For large-scale motions, the equations of motion can be simplified by making the hydrostatic and Boussinesq approximation and are written for the ocean

$$du/dt - fv + p_x / \rho_o = F^x \quad (6)$$

$$dv/dt + fu + p_y / \rho_o = F^y \quad (7)$$

$$p_z + \rho' g = 0 \quad (8)$$

$$u_x + v_y + w_z = 0 \quad (9)$$

$$d\rho / dt = G \quad (10)$$

where z is positive upwards, ρ_o is the reference density and ρ' the density departure from ρ_o , p is the pressure, and the terms F and G represent the body forces, dissipative processes and heat sources. The curvature of the earth enters the equations through the Coriolis parameter $f = \beta y$, where $\beta = 2\Omega/a$ is equal to $2.3 \cdot 10^{-11} \text{ m}^{-1} \text{ s}^{-1}$ and a is the earth radius. In the atmosphere, compressibility should be taken into account, as discussed later. To linearize these equations, we consider a motionless basic state with density $\bar{\rho}(z)$ a function of depth only, with $\rho' = \bar{\rho}(z) + \rho(x, t)$. In the inviscid unforced case, small perturbations to this basic state obey

$$u_t - fv + p_x / \rho_o = 0 \quad (11)$$

$$v_t + fu + p_y / \rho_o = 0 \quad (12)$$

$$p_z + \rho g = 0 \quad (13)$$

$$u_x + v_y + w_z = 0 \quad (14)$$

$$\rho_t - N^2 \rho_o w / g = 0 \quad (15)$$

where $N = (-g\bar{\rho}_z / \rho_0)^{1/2}$ is the Brunt-Väisälä frequency, and ρ denotes the density perturbation.

With a flat bottom at depth H , the boundary conditions for the ocean are

$$w = 0 \quad \text{at } z = -H \quad (16)$$

$$w = p_t / \rho_0 g \quad \text{at } z = 0$$

For the atmosphere, a radiation condition is more appropriate. Eliminating ρ between (13) and (15) yields

$$w = -\frac{1}{\rho_0 N^2} P_{zt}$$

Replacing in (14) gives

$$u_x + v_y - \frac{1}{\rho_0} (N^{-2} p_{zt})_z = 0 \quad (17)$$

This system of equations can be solved by a separation of variables. Assuming that

$$\begin{aligned} u &= \tilde{u}(x, y, t) R(z) \\ v &= \tilde{v}(x, y, t) R(z) \\ p &= \rho_0 \tilde{\pi}(x, y, t) R(z) \\ w &= \tilde{w}(x, y, t) S(z) \end{aligned} \quad (18)$$

leads to

$$(N^{-2} R_z)_z / R = -(gh)^{-1} = \frac{\tilde{u}_x + \tilde{v}_y}{\tilde{\pi}_t} \quad (19)$$

where h is the constant of separation (the equivalent depth), and with

$$R = -ghS_z \quad \text{and} \quad S = N^{-2}R_z \quad (20)$$

The oceanic boundary conditions become

$$R_z = 0 \quad \text{at } z = -H \quad (21)$$

$$R + gR_z/N^2 = 0 \quad \text{at } z = 0 \quad (22)$$

b Normal modes. Equation (19) describes the vertical structure of the motion, and it can be solved in a number of different ways. The most convenient for many tropical ocean problems is based on a representation in terms of vertically standing modes. Together with (21) and (22), Eq. (19) represents a Sturm-Liouville problem. For continuous stratification, there are an infinite set of discrete solutions (eigenmodes) R_n corresponding to discrete values of the equivalent depth

(eigenvalues) h_n , where h_n increases with the vertical mode index $n = 0, 1, 2, \dots$. The eigenmodes are orthonormal and form a complete set, so that any motion or forcing can be expressed as a sum of the vertical modes. In the atmosphere, a better representation is in terms of vertically propagating modes. However, in atmospheric models one often assumes that there is a rigid lid at the top of the troposphere or the stratosphere, and vertical standing modes may provide an useful representation.

For realistic density profils, the eigenmodes and eigenvalues must be calculated numerically, although the barotropic mode $n = 0$, for which $h_0 \approx H$, is unaffected by the stratification and can be calculated analytically. However, the latter cannot be properly represented on the equatorial β -plane and anyway is of little relevance to the tropical oceans. The baroclinic modes cause little vertical elevation of the free surface, and they are often calculated assuming a rigid lid. As the vertical mode number increases, the number of nodes increases (voir figure ci-dessous, de Philander, 1990). Typical values for the equivalent depths in the ocean are $h_1 = 60$ cm, $h_2 = 20$ cm... For the atmosphere, Gill (1980) uses $h_1 = 500$ m.

The horizontal and time dependence of mode n is given by (omitting the index n)

$$\tilde{u}_t - f\tilde{v} + \tilde{\pi}_x = 0 \quad (23)$$

$$\tilde{v}_t + f\tilde{u} + \tilde{\pi}_y = 0 \quad (24)$$

$$\tilde{\pi}_t + c^2(\tilde{u}_x + \tilde{v}_y) = 0 \quad (25)$$

where $c = (gh)^{1/2}$ is the gravity wave speed. If \tilde{v} is different from zero, these equations can be reduced to a single equation for the meridional velocity component \tilde{v}

$$(\tilde{v}_{xx} + \tilde{v}_{yy})_t + \beta\tilde{v}_x - \frac{1}{c^2}(\tilde{v}_{tt} + \beta^2 y^2 \tilde{v})_t = 0 \quad (26)$$

If the indice n characterizing the vertical mode number is now written explicitly, zonally propagating wave solutions have the form

$$\tilde{v}_n = V_n(y) e^{i(kx - \omega t)} \quad (27)$$

where the horizontal structure obeys

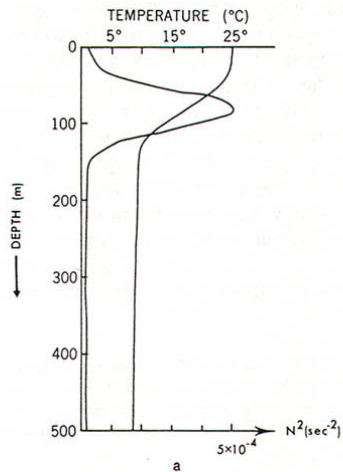
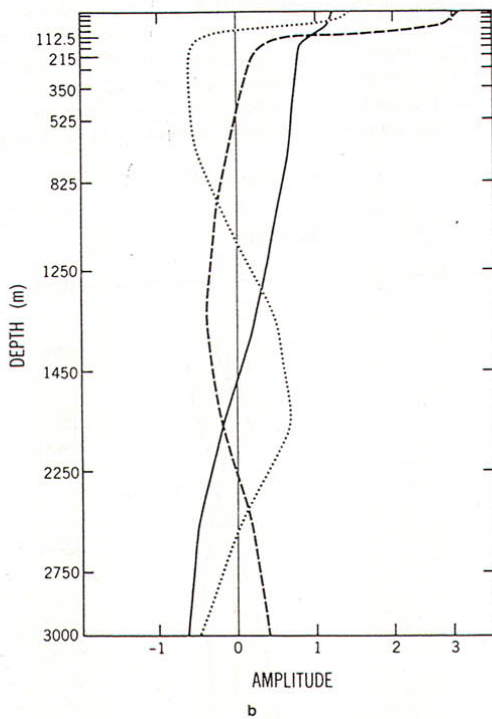


Figure 4.1. (a) A representative profile of the temperature and Brunt–Väisälä frequency in the tropics. This profile, with the temperature decreasing linearly to zero below 500 m, is used as initial condition in the model that provides the results in Figs. 4.5 to 4.9 and 4.16. (b) The structure of the three gravest vertical modes associated with the stratification in (a).



$$d^2V_n/dy^2 + (\omega^2/c_n^2 - k\beta/\omega - k^2 - \beta^2y^2/c_n^2)V_n = 0 \quad (28)$$

Solutions of (28) are oscillatory equatorward of the critical latitudes defined by

$$y_{nc} = \pm (\omega^2/\beta^2 - kc_n^2/\beta\omega - k^2c_n^2/\beta^2)^{1/2} \quad (29)$$

and exponentially decaying poleward of y_{nc} .

Equation (26) can be used to define characteristic equatorial scales. A meridional length scale is obtained by considering the balance between \tilde{v}_{yyt} and $c^{-2}\beta^2y^2\tilde{v}_t$, yielding the equatorial radius of deformation $L_n = (c_n/\beta)^{1/2}$, which is of the order of 300km for the lowest baroclinic oceanic mode. For $|y|$ larger than L_n , the Coriolis term dominates, as in the mid latitudes, and for $|y|$ smaller, it becomes negligible, so that L_n determines the width of the distinctive equatorial zone. The time scale $T_n = (c_n\beta)^{-1/2}$ determines the relative importance of \tilde{v}_t and $\beta^2y^2\tilde{v}$, and is the time it takes to form a distinctive equatorial zone, which is the inertial time at latitude L_n ($L_I \approx 1.5$ days). The non-dimensionalization leads to a canonical form of (28) that is the same for all vertical modes

$$d^2V/dy^{*2} + (\omega^{*2} - k^{*2}/\omega^{*2} - k^{*2} - y^{*2}) V = 0, \quad (30)$$

where the asterisk indicates nondimensional variables, and the index n has again been omitted. The wave solutions of equation (30) can either be represented as latitudinally propagating wave packets that are refracted at the critical latitude y_c^* and thus equatorially trapped (see Philander 1990), or as standing latitudinal modes. The latter modes, described below, are evanescent poleward of the turning latitude, and known as equatorially trapped modes.

Bounded solutions at large values of $|y^*|$ are only possible for the eigenvalues given by

$$\omega^{*2} - k^{*2}/\omega^{*2} - k^{*2} = 2m + 1, \quad m = 0, 1, 2, \dots \quad (31)$$

which defines the dispersion relation of the equatorially trapped modes (Fig.22). The modes are orthonormal and given by

$$V_m = \pi^{1/4} (2^m m!)^{-1/2} H_m(y^*) \exp(-y^{*2}/2) \quad (32)$$

where $H_m(y)$ is the m^{th} Hermite polynomial. The Hermite polynomials are defined by

$$H_m(y) = (-1)^m e^{y^2} \frac{d^m}{dy^m} e^{-y^2}$$

and the first ones are: $H_0=1$, $H_1=2y$, $H_2=4y^2 - 2$, ... The even modes are symmetric about the equator, the odd modes antisymmetric. As sketched in Fig.23, the critical latitude y_c^* increases

with the latitudinal mode number. However, it decreases with the vertical mode number, as shown by the dimensional form

$$y_{nm} = (c_n (2m + 1)/\beta)^{1/2} = L_n (2m + 1)^{1/2} \quad (33)$$

Typical values in the ocean are $y_{11c} = 325$ km, $y_{21c} = 250$ km,... Note that $y_{01c} = 3000$ km is too large for the equatorial β -plane approximation to be valid, as noted before.

As the modes form complete sets, the general solution of the linearized equations can be represented by an expansion of the form

$$v = \sum_n \sum_m v_{nm}, u = \sum_n \sum_m u_{nm}, \frac{p}{\rho_0} = \sum_n \sum_m \pi_{nm} , \quad (34)$$

with

$$v_{nm} = A_{nm} R_n(z) V_m(y/R_n) \cos(kx - \omega t), \quad (35)$$

where the amplitude A_{nm} is determined by the initial and boundary conditions. To derive the zonal velocity, $\tilde{\pi}$ is eliminated between (23) and (25), yielding

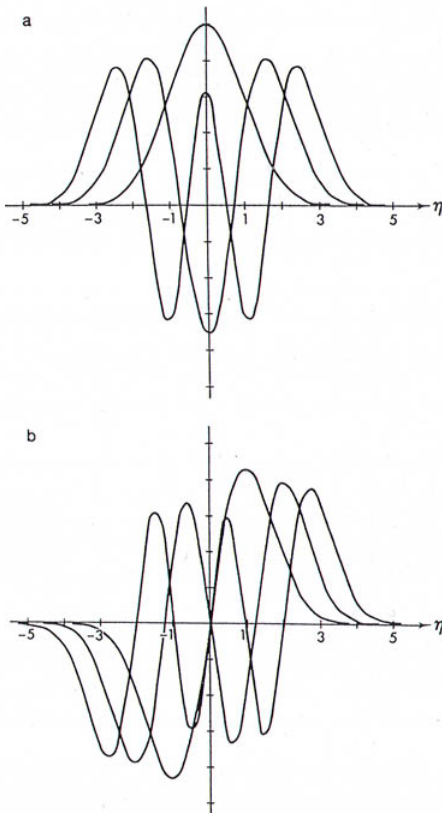


Figure 3.9. The latitudinal structure of (a) symmetrical and (b) antisymmetrical Hermite functions that describe the meridional velocity component. The unit of distance in the northward direction is the equatorial radius of deformation.

$$\tilde{u}_t - c^2 \tilde{u}_{xx} = b y \tilde{v}_t + c^2 \tilde{v}_{xy} \quad (36)$$

After substituting (34) and (35), recurrence relations for the Hermite polynomials lead to

$$u_{nm} = -0.5 A_{nm} R_n(z) (a_{nm} V_{m+1}(y/L_n) + b_{nm} V_{m-1}(y/L_n)) \sin(kx - \omega t) \quad (37)$$

$$\pi_{nm} = -0.5 c_n A_{nm} R_n(z) (a_{nm} V_{m+1}(y/L_n) - b_{nm} V_{m-1}(y/L_n)) \sin(kx - \omega t) \quad (38)$$

with $a_{nm} = (2(m+1)\beta c_n)^{1/2}/(\omega - kc_n)$ and $b_{nm} = (2mc_n\beta)^{1/2}/(\omega + kc_n)$. Note the different parity of the Hermite polynomials entering (36) and (37): when the meridional velocity is symmetric about the equator, the zonal velocity and the pressure are antisymmetric, and vice-versa.

c *The different types of waves.* In dimensional form, the dispersion relation (31) takes the form

$$\omega^2/c_n^2 - k\beta/\omega - k^2 = (2m + 1)\beta/c_n, \quad n = 1, 2, 3, \dots \text{ and } m = 0, 1, 2, \dots \quad (39)$$

and it admits different types of wave solutions: mixed Rossby-gravity waves (or Yanai wave), Rossby waves and inertia-gravity waves.

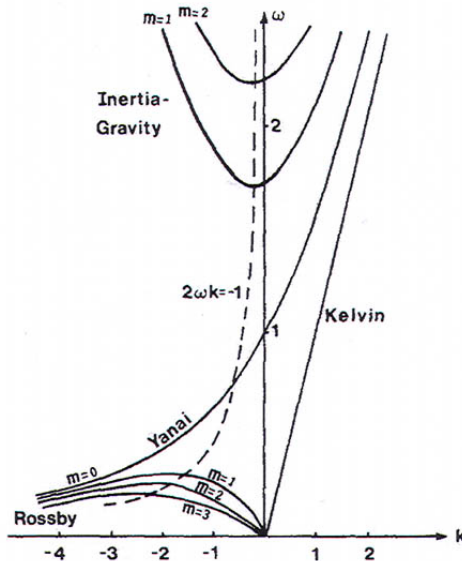


FIG. 1. The dispersion relation for equatorial waves. The minimum frequency for the inertia-gravity wave modes occurs for the $m = 1$ mode at $k = -1/2\omega$ and is $1 + 2^{-1/2}$. The maximum frequency for the Rossby wave modes occurs for the $m = 1$ mode at $k = -1/2\omega$ and is $1 - 2^{-1/2}$.

The mixed Rossby-gravity waves is the gravest mode, corresponding to $m = 0$, so that $V_{n0} \propto H_0 \propto \exp(-\beta^2 y^2 / 2c_n)$ (cross-equatorial flow) and $U_{n0} \propto H_1$ (zonal flow of opposite sign across the equator. Then, (39) can be written

$$(\omega/c_n + k)(\omega/c_n - \beta/\omega - k) = 0 \quad (40)$$

The first root must be discarded because the associated zonal velocity becomes unbounded for increasing y , so the dispersion relation reduces to

$$\omega/c_n - \beta/\omega - k = 0 \quad (41)$$

Hence, the mixed Rossby-gravity wave is similar to a (short) Rossby wave at low frequencies and to a gravity wave at high frequencies (Fig. 3.8).

For $m = 1, 2, 3, \dots$ there are two roots at each frequency

$$k = -\beta/2\omega \pm (\beta^2/4\omega^2 + \omega^2/c_n^2 - (2m+1)\beta/c_n)^{1/2} \quad (42)$$

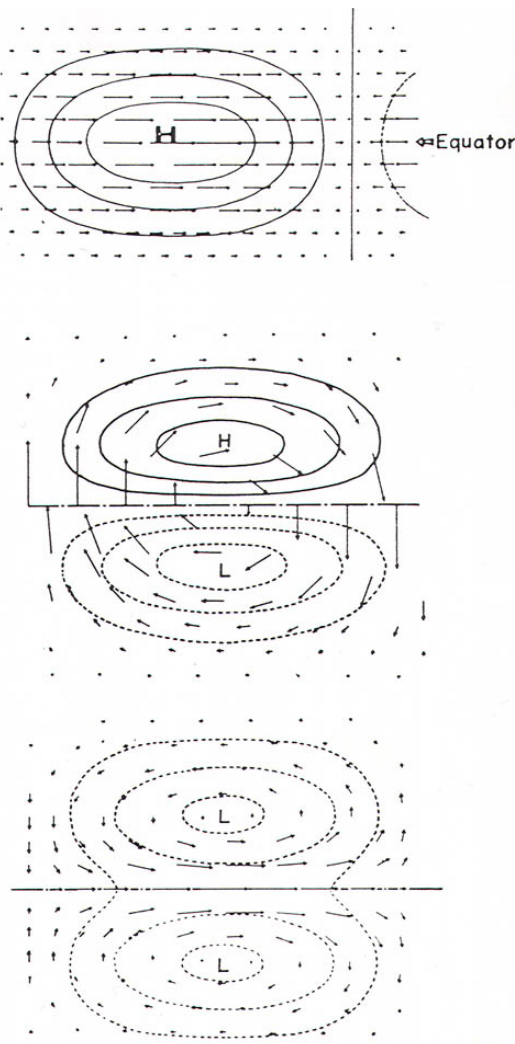


FIG. 5. Pressure and wind fields associated with several basic modes of equatorial waves (after Matsuno, 1966): top, Kelvin wave ($n = -1$); middle, mixed Rossby-gravity wave ($n = 0$); bottom, the lowest mode Rossby wave ($n = 1$).

There is a frequency interval when the argument of the square root is negative and the zonal wavenumber k becomes complex; this corresponds to periods between about 5 and 30 days. At

high frequencies, the solutions are the inertia-gravity waves. At low frequencies, the dispersion relation (42) simplifies to

$$\omega = -\beta k / (k^2 + (2m+1)\beta/c_n) \quad (43)$$

which describes the equatorially trapped Rossby modes. For $m = 1$, v is antisymmetric with respect to equator, while u and p are symmetric. Noteworthy is that the frequency gap between Rossby and gravity waves is much smaller near the equator than in the mid-latitudes.

As in the mid-latitudes, the phase velocity of the Rossby waves is always westwards, and their group velocity c_g is westwards for the long waves and eastwards for the short waves. At very low frequencies, the long non dispersive Rossby waves, which play a crucial role in the oceanic adjustment to changes in the wind stress, have a much larger zonal than meridional velocity. They propagate rapidly, with group velocity given by $c_g = -c_n/(2m+1)$, which is about 0.8 m/s for the gravest meridional and vertical mode in the ocean. This is much faster than in the mid-latitudes. The short Rossby waves are much slower, having an eastward group velocity that is at most 8 time smaller than the propagation speed of the long non-dispersive waves. The short Rossby waves are thus more easily dissipated, but they play an important role in the adjustment problem near the western boundary. It is easy to show that, at low frequencies, the horizontal motion of the short Rossby waves is nondivergent, so that the waves are not associated with a net zonal mass flux. Thus, these waves cannot redistribute mass zonally.

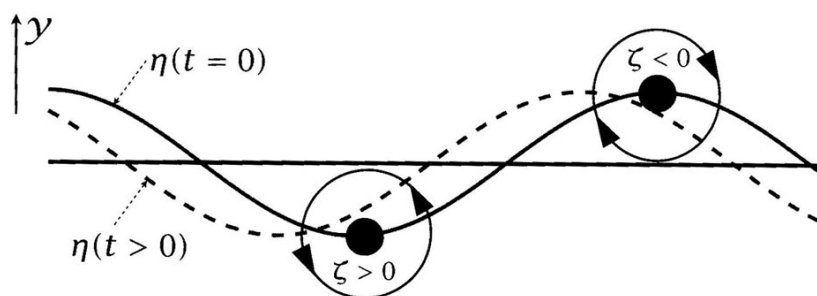


Fig. 5.4 The mechanism of a two-dimensional (x - y) Rossby wave. An initial disturbance displaces a material line at constant latitude (the straight horizontal line) to the solid line marked $\eta(t = 0)$. Conservation of potential vorticity, $\beta y + \zeta$, leads to the production of relative vorticity, as shown for two parcels. The associated velocity field (arrows on the circles) then advects the fluid parcels, and the material line evolves into the dashed line. The phase of the wave has propagated westwards.

There is an additional wave solution that has no meridional velocity, the equatorial Kelvin wave. If $v=0$, the system (23)-(25) simplifies to

$$\tilde{u}_t + \tilde{\pi}_x = 0 \quad (44)$$

$$f\tilde{u} + \tilde{\pi}_y = 0 \quad (45)$$

$$\tilde{\pi}_t + c^2 \tilde{u}_x = 0 \quad (46)$$

which yields

$$\tilde{u}_{tt} - c^2 u_{xx} = 0 \quad (47)$$

$$\beta y \tilde{u}_t - c^2 \tilde{u}_{xy} = 0 \quad (48)$$

For a propagating solution of the form

$$\tilde{u} = E(y) e^{i(kx - \omega t)} \quad (49)$$

relation (47) gives the relation dispersion

$$\omega = k c, \quad (50)$$

where only the positive solution is given as the negative one is associated with unbounded values at large y , as shown by (50) which yields

$$E(y) = A \exp(-\omega \beta y^2 / 2kc^2) = A \exp(-\beta y^2 / 2c^2) \quad (51)$$

where A is a constant. The non-dispersive Kelvin wave solution is thus given by

$$u = F(x - c_n t) \exp(-y^2 / L_n^2), \quad (52)$$

where F is an arbitrary function. The Kelvin wave is trapped near the equator, and it propagates eastward at the gravity wave speed c_n that is three times larger than the group velocity of the fastest Rossby waves. The crossing time for the equatorial Pacific Ocean is only of the order of 2 months for the gravest modes.

The relation between u and p can be derived from (44) and (50), yielding $\tilde{\pi} = c\tilde{u}$, so that u is in phase with p . For a first baroclinic mode, u is also in phase with the sea surface elevation

and out of phase with the thermocline displacement. A first baroclinic mode that is excited by a westerly wind stress burst is a downwelling Kelvin wave. Westerly wind bursts frequently occur over the western Pacific warm pool, hence the resulting Kelvin waves advect warm water eastwards and at the same time depress the thermocline, reducing the efficiency of equatorial sea surface temperature cooling by upwelling. Both effects add and may create anomalous sea surface temperature warming in the central and eastern Pacific, as discussed below.

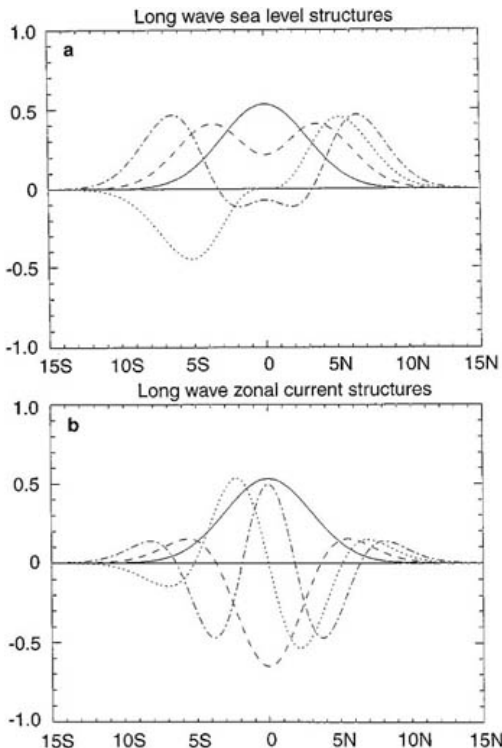


Fig. 1a, b Meridional structures of **a** sea level and **b** zonal current (calculated for a 2.5 m/s Kelvin phase speed). Each wave amplitude at a given latitude can be obtained by multiplying the meridional structure to the calculated coefficient, yielding for cm or cm/s for TOPEX/POSEIDON sea level anomaly coefficients or N/m² for ERS wind stress anomaly coefficients

The structure of Kelvin and long Rossby waves is illustrated in Fig. 1a,b (from Boulanger and Menkes, Climate Dynamics 1999) and their evolution in Fig. 24 by the dispersion of an initially bell-shaped thermocline displacement in a two-layer model. The figure emphasizes that these non-dispersive waves generally resemble pulses rather than sinusoids, and it nicely shows some of their characteristic features. The zonal current associated with a first meridional Rossby mode has a maximum at the equator and changes sign a few degrees from it, while the thermocline displacement has a minimum at the equator but no change in sign. On the contrary, the two variables are exactly out-of-phase for the Kelvin wave, with maximum amplitude at the

equator. As predicted, observations at the equator show that, at low frequencies, the zonal current fluctuations are much more energetic than the meridional ones.

d Reflections at meridional boundaries. The reflection of an incident wave at a solid boundary is solved by assuming that it creates a reflected perturbation, often in the form of waves, that cancels the velocity normal to the boundary at all time and depth along the boundary. For example, at a meridional boundary, it is assumed that the zonal velocity consists of that of the incident wave u^i plus a reflected component u^r . The boundary condition at $x = L$, say, is $u^i + u^r = 0$ for all t , z , and y . The first two conditions impose that the vertical structure and the frequency of the reflected perturbation are those of the incident wave, while the third one constraints its nature.

The complexity of equatorial wave reflections is easily understood from the dispersion diagram in Fig. 3.8. At low frequencies, the diagram is very asymmetrical about the $k=0$ axis, and at intermediate frequencies near $(\beta c)^{1/2}$, there is a frequency gap where waves can propagate energy eastwards but not westwards (the group velocity is given by the slope of the dispersion curves). In this frequency gap, Kelvin or Rossby-gravity waves impinging an eastern boundary cannot excite westward propagating waves, and energy accumulates at the eastern side. However, (42) shows that wave solutions with a complex zonal wavenumber can exist in the presence of a meridional coast, so in fact the incoming waves excite coastally trapped waves. It can be shown (Moore 1968) that these disturbances propagate poleward and that, far from the equator, their sum asymptotes to a single wave that resemble a coastal Kelvin wave. Therefore, the energy of the equatorially trapped waves leaks poleward along the eastern boundary.

As the frequency of the incoming wave decreases, an increasing number of westward propagating long Rossby waves become available for reflection. Consider an incident Kelvin wave, which has a zonal velocity with a V_0 meridional structure. To satisfy the boundary condition $u=0$ at the eastern boundary, a number of Rossby modes of odd parity (for symmetry reason) are available, and it is easy to see how their amplitude can be determined. The amplitude of the $m=1$ mode is chosen to exactly cancel the V_0 Kelvin wave signal, but then the superposition of the two waves has a V_2 structure that needs to be cancelled, as shown by (37). This is done by a proper choice of the amplitude of the $m=3$ mode, if it is available, but the latter introduces a V_4 structure, and so on. An infinite set of Rossby modes would be needed to satisfy the boundary condition, but except for very low frequencies, only the first few modes are available and a portion of the reflected signal remains trapped near the coast. The latter

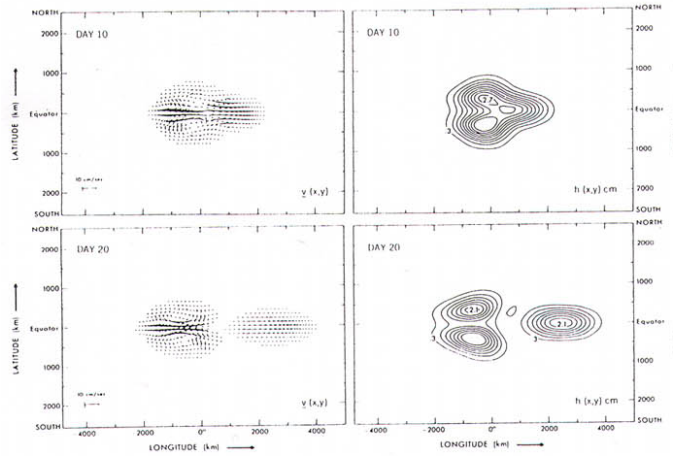


Fig. 24. The dispersion of an initially bell-shaped thermocline displacement into an eastward-propagating Kelvin wave and westward-propagating Rossby waves. The left-hand panels show the horizontal currents and the right-hand panels the thermocline displacements. (From Philander et al. 1984).

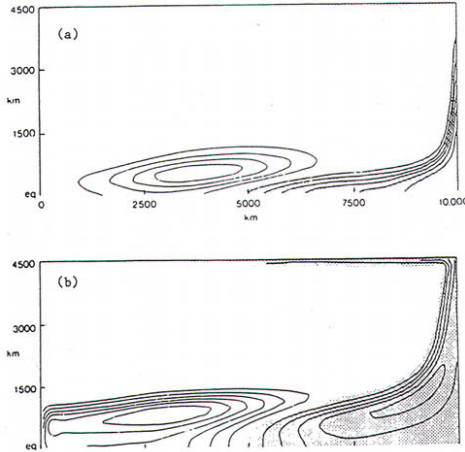


Figure 1. Evolution of thermocline depth in a linear shallow water model following sudden switch-on of a localized wind patch in midbasin. (a) 3 months and (b) 13 months. Months are dimensioned using wave speeds characteristic of the first baroclinic mode. After McCreary and Anderson [1984].

corresponds to solutions with complex zonal wavenumber, and as before energy is propagated poleward by the coastally trapped waves, which again asymptote far from the equator to a coastal Kelvin wave-like solution. The energy leakage toward the midlatitudes decreases as more Rossby modes become available for reflection, and in the limit of vanishing frequency the leakage becomes negligible (Fig. 2 de Clarke JPO 2003). It can be shown that at very low frequencies, $1/2$ of the Kelvin wave energy flux is reflected as a first Rossby mode, $1/8$ as a second mode, $1/16$ as a third mode, and so on (Clarke 1983). As the higher meridional modes are less trapped near the equator (rel. (33)) and propagate more slowly, the reflection at the eastern boundary increases the width of the disturbances, more rapidly so near the equator.

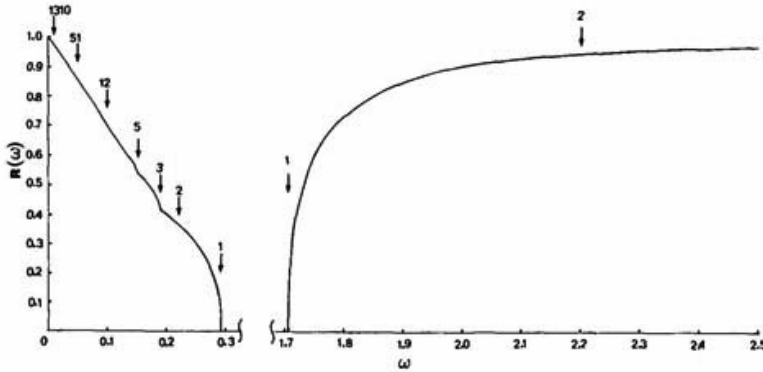


FIG. 2. The energy flux reflection coefficient of an equatorial Kelvin wave reflecting from an eastern meridional boundary. The graphs intersect the ω axis at $\omega = 1 - 2^{-1/2}$ and $\omega = 1 + 2^{-1/2}$, the frequencies corresponding to the highest frequency for equatorial planetary wave modes and the lowest frequency for inertia gravity wave modes. For $1 - 2^{-1/2} < \omega < 1 + 2^{-1/2}$ no waves with westward group velocity away from the boundary exist and $R(\omega) = 0$. For ease of plotting, the ω axis is broken between $\omega \approx 0.3$ and $\omega \approx 1.7$. The arrows and associated numbers point to the frequency when that number mode (planetary or inertia gravity) becomes available for reflection

$$\left[\omega = \left(\frac{m+1}{2} \right)^{1/2} - \left(\frac{m}{2} \right)^{1/2} \text{ or } \left(\frac{m+1}{2} \right)^{1/2} + \left(\frac{m}{2} \right)^{1/2}, \text{ respectively} \right].$$

The reflection at the western boundary is different because (symmetric) Kelvin or (antisymmetric) Rossby-gravity waves are always available to propagate energy eastward, so that there is no poleward loss of energy. The same argument than above can be used to determine the amplitude of the reflected waves. Consider an incident long Rossby wave with meridional mode number m . The zonal velocity has meridional structures $m+1$ and $m-1$, which have to be cancelled at the meridional boundary. Canceling the $m+1$ structure with a short Rossby wave of meridional mode number m specifies the amplitude of the short wave, but leaves a non-zero $m-1$ structure. This, however, can be cancelled by a short $m-2$ Rossby mode, and the resulting $m-3$ structure by a $m-4$ mode, and so on, until a Kelvin or a Rossby-gravity mode, depending on symmetry, is introduced to close the problem. As waves with meridional mode number smaller or equal to that of the incident wave are involved, the reflected signal is at least as equatorially trapped as the incident one.

It has been mentioned that, at very low frequencies, the short Rossby waves cannot induce any net zonal mass transport. Hence, they are unable to return the zonal mass flux that is associated with an incoming symmetric Rossby wave (there is no net zonal mass flux for antisymmetric waves). Consequently, the mass flux must be returned eastward by the Kelvin wave, which directly determines its amplitude (Cane and Sarachik 1977). For the gravest $m=1$ Rossby mode, one half of the energy is reflected as a Kelvin mode, while for higher meridional modes the fraction is much smaller (Fig.4 de Clarke JPO 2003). When the reflected Kelvin wave reaches an eastern boundary, it is again reflected as described above. It can be shown that in closed ocean basins with idealized geometry, "slightly leaky" resonant basin modes that only

involve an equatorial Kelvin wave and long Rossby waves are possible (Cane and Moore 1981). Such modes are indeed observed during the spin-up of simplified ocean models.

Ocean boundaries are not meridional, however, and there have been various attempts at performing calculations with more realistic boundaries. In particular, the influence of inclined boundaries and coastal gaps as found in the western Pacific has been investigated. The effect of tropical islands on wave propagation has also been considered. The results suggest some differences with the idealized cases, for example a Kelvin wave can also be excited at a non-meridional western boundary by an antisymmetric long Rossby wave, but, in general, the gravest modes seem to be little affected.

f. Forcing. The tropical oceanic fluctuations are primarily wind-driven, either at the boundaries or in the mid-ocean when the trade winds relax or strengthen. If the wind stress τ acts as a body force in a surface layer of depth h , the forcing in (6) and (7) is

$$\mathbf{F} = \tau Z(z)/\rho_0 h, \quad (53)$$

where $Z(z) = 1$ if $-h \leq z \leq 0$, and zero otherwise. In the normal mode representation, the body force can be expanded in terms of the vertical eigenfunctions

$$Z(z) = \sum_{n=1}^{\infty} Z_n R_n(z) \quad (54)$$

with

$$Z_n = \int_{-h}^0 R_n(z) Z(z) dz \quad (55)$$

The forcing can also be expanded in terms of the Hermite functions, so that the response of each mode can be computed separately. The atmospheric response to diabatic heating can be treated similarly, as discussed below.

e. Influence of the mean flow. The solutions above are valid for a motionless basic state. However, both in the atmosphere and the ocean, the mean flow is important and has a complex structure. The meridional section of the zonal geostrophic current (a good approximation under the surface layer) below shows the strong vertical and horizontal shear of the equatorial current system in the Pacific. The interaction of the waves with the mean shear currents is measured by the ratio of the speed of the wave to that of the mean current. It has a significant influence on the vertical profile of the equatorial waves of low mode number, while affecting less their

propagation speed (e.g., McPhaden and Ripa 1990). This needs not be discussed here, but is illustrated below for the Kelvin wave in the presence of a simplified current system. Note the large velocity maximum below the surface. On the other hand, the properties and the propagation of the slower, higher modes are strongly modified (Philander 1990).

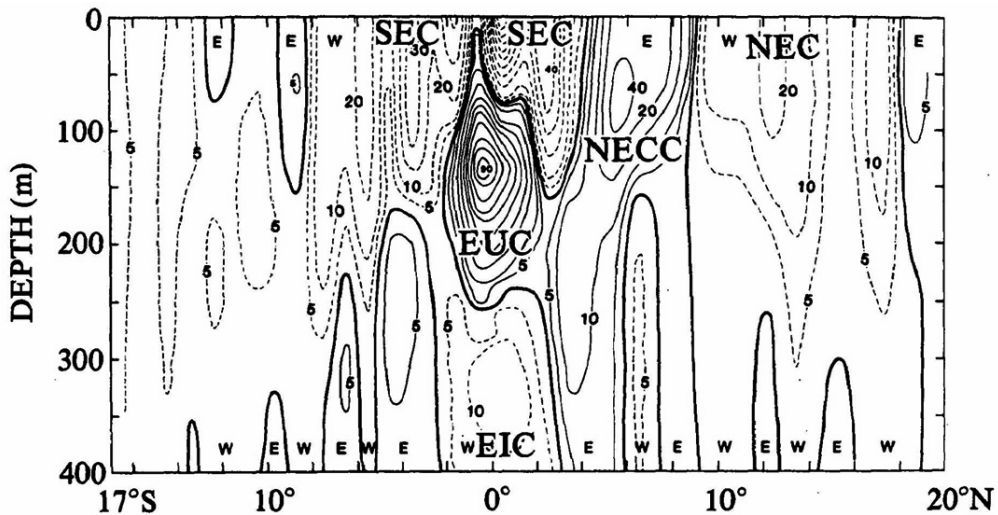
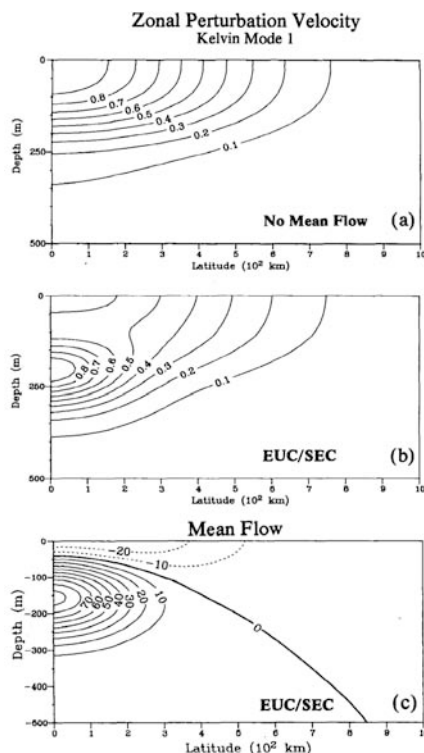


Figure 2 Contours of geostrophic zonal velocity (in centimeters per second) derived from conductivity-temperature-depth data collected during the Hawaii-Tahiti Shuttle Experiment (from Wyrtki & Kilonsky 1984). Shown is the mean averaged across 150°W – 158°W for February 1979–June 1980 based on 15 quasi-monthly cruises. Solid (dashed) contours indicate eastward (westward) flow. Currents indicated are the Equatorial Undercurrent (EUC), the South Equatorial Current (SEC), the North Equatorial Current (NEC), North Equatorial Countercurrent (NECC), and the Equatorial Intermediate Current (EIC).



f Observations. Since the 80s, there has been growing observational evidence that Kelvin and Rossby waves are common in the equatorial oceans and play an important role in ENSO and

other low frequency fluctuations. Only the lowest vertical modes have been detected, in part because the observations are usually noisy, but also because of non-linearities and the interaction of the waves with the mean shear currents. Eastward propagating pulses in sea level, thermocline depth and zonal current with Kelvin wave-like properties are generated by the strong westerly wind bursts that frequently occur in the western Pacific. Such a wind event was observed in May 1986 (Fig.28), lasting about 10 days. The ocean showed a strong local response with a large sea level elevation and a 25 m thermocline deepening; eastward currents exceeding 1 m/s were observed down to a depth of 100 m. Sea level observations along the equator and at coastal stations document the subsequent eastward propagation of the Kelvin wave like pulse across the entire equatorial Pacific, reaching the American coast about 45 days later (Fig.29). Although the peak becomes less recognizable as the wave crosses the basin, the propagation speed was estimated to be about 3m/s, slightly faster than the speed of a first baroclinic mode.

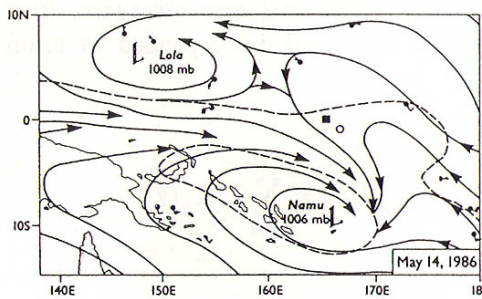


Fig. 28. Surface streamline analysis for May 14, 1986. The dashed line is the 15 knot (1 knot = 0.5 m/s) isotach. Full (half) bars on wind arrows indicate 10-knots (5-knots) speed increments. Tropical cyclones Namu and Lola formed on May 15 and 17, respectively, in the low-pressure centers straddling the equator. (From McPhaden et al. 1988).

Better-documented cases have been found in the altimetric observations. Here we reproduce some of the analysis of the GEOSAT-derived sea level and zonal current anomalies by Delcroix et al. 1994, which nicely show the influence of wind forcing, wave propagation and reflection at the boundaries from November 1986 to February 89. The interpretation was greatly facilitated by projecting the data onto the (first baroclinic) Kelvin mode and the gravest Rossby modes. As shown in the figure, the Kelvin mode and the first symmetric Rossby mode explain most of the variance of the zonal current anomalies. Note that the wave field is quite complex because wind forcing continuous acts on the ocean, so that wind events in the middle of the basin or near its boundaries generate new waves that interfere with the existing ones, and at time mask the reflection of the latter. However, this can be modeled successfully by projecting the forcing onto the various modes, as illustrated for the Kelvin wave, and estimating the oceanic response. A strong westerly wind anomaly located west of 170°W first generated a downwelling Kelvin

wave that propagated across the entire Pacific at about 3 m/s and may have been associated with the initiation of the 1986-1987 El Niño. Note also the upwelling Kelvin wave-like perturbation that is related to the easterly wind stress anomaly in February 1987, and the series of downwelling Kelvin waves in March-October 87. A strong downwelling Rossby wave is seen from March to September 1987, consistent with the wind forcing during this period (not shown), followed by two upwelling Rossby waves forced by the wind in the eastern Pacific. These waves switched the zonal current anomaly to westward and contributed to the termination of the 86-87 El Niño. Then, the 1988-89 La Niña is characterized by upwelling Kelvin waves related to the enhancement of the trade winds in the western part of the basin, which maintain westward zonal currents for more than a year.

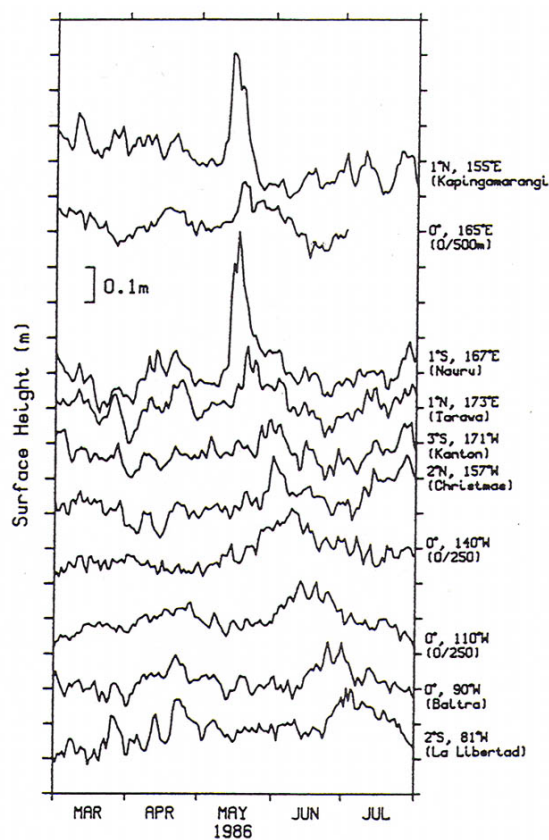


Fig. 29. Time series of sea level from island and coastal stations, and surface dynamic height (related to indicated reference levels) from moorings between 2°N and 2°S. (From McPhaden et al. 1988).

Wave reflections at the boundaries have been detected in the altimetric data. They are best seen below in the time evolution of the Kelvin and Rossby wave part of the signal, obtained as before by projection onto their respective meridional structure. This is illustrated for the Kelvin wave and first meridional Rossby modes, using the TOPEX-POSEIDON data (Boulanger and Menkes 1999). There is clear evidence of Kelvin wave reflection into Rossby modes at the

eastern boundary, and a detailed calculation suggests that the reflection efficiency of the South American coast is about 75% of that of an infinite meridional wall for the first meridional Rossby mode. Similar results (65%) were found for the third meridional Rossby mode. The reflection of the Rossby waves into Kelvin waves at the eastern boundary is harder to see because the reflected Kelvin wave signals are masked by the large amplitude Kelvin waves forced by the wind in the western part of the basin. Nonetheless, during the strong 1997-98 El Niño event when the upwelling Rossby wave was large, the reflected Kelvin wave signal propagated east of the dateline, but it was partially cancelled there by wind-forced downwelling Kelvin waves. Because of the changing wind forcing, displays are difficult to interpret but a more quantitative analysis suggested high reflection efficiency.

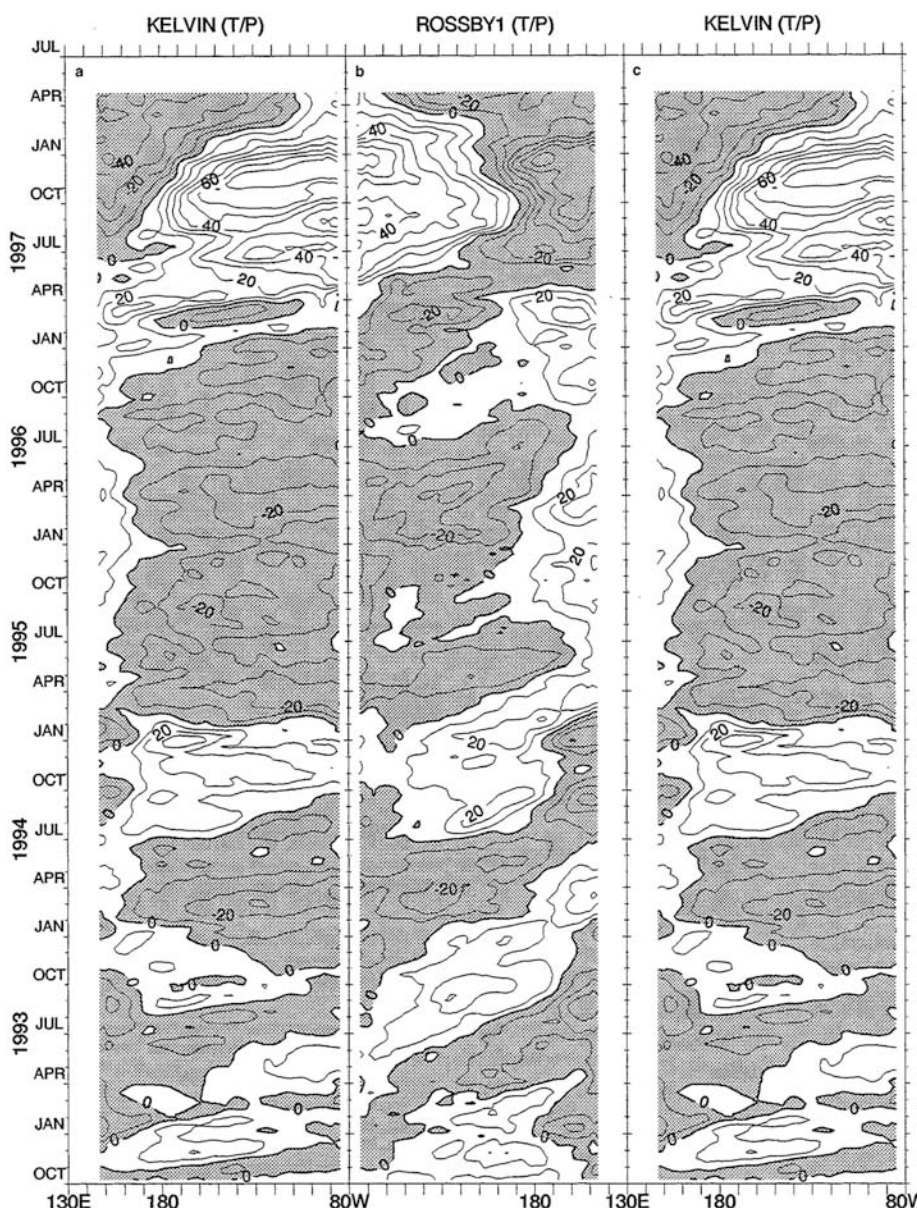


Fig. 6 a longitude-time plots of the TOPEX/POSEIDON Kelvin wave coefficient (from 130°E to 80°W; repeated for comparison). b the first-mode Rossby wave coefficient (in reverse display from 80°W to 130°E), and c the Kelvin wave coefficient (from 130°E to 80°W; repeated for comparison). Contour interval is 10 units for both coefficients. Positive (negative) coefficients are white (gray)